

LASER INTERFEROMETER GRAVITATIONAL
WAVE OBSERVATORY
- LIGO -

CALIFORNIA INSTITUTE OF TECHNOLOGY
MASSACHUSETTS INSTITUTE OF TECHNOLOGY

Document Type **LIGO-T990075-00-D** August 16, 1999

**Proposal of a Seismic Attenuation System (SAS)
for the LIGO Advanced Configurations (LIGO2)**

Mark Barton, Alessandro Bertolini, Eric Black, Giancarlo Cella, Eugene W. Cowan,
Erika D'Ambrosio, Riccardo DeSalvo, Ken Libbrecht, Virginio Sannibale,
Akiteru Takamori, Nicolas Viboud, Phil Willems and Hiroaki Yamamoto

Distribution of this draft:
SEI group

This is an internal working note
of the LIGO Project.

California Institute of Technology	Massachusetts Institute of Technology
LIGO Project - MS 18-34	LIGO Project - MS 20B-145
Pasadena, CA 91125	Cambridge, MA 01239
Phone (626) 395-2129	Phone (617) 253-4824
Fax (626) 304-9834	Fax (617) 253-7014
E-mail: info@ligo.caltech.edu	E-mail: info@ligo.mit.edu

WWW:<http://www.ligo.caltech.edu/>

1 Introduction

The SAS is basically a passive system capable of isolating the LIGO2 test masses from seismic noise bringing it well below the mirror's thermal noise level, starting from frequencies comparable with the gravity gradient wall.

The SAS active components will be used to reduce the off-band test mass residual rms movement. The reduction of rms noise will reduce the mirror actuator required dynamic range with the aim to allow advanced mirror control (photon drive on the final mirror control instead of the electrostatic or electromagnetic ones).

The main SAS desired features are the following:

1. The in-band passive attenuation capability sufficient to overkill and maintain the seismic noise in all dof well below the thermal noise limit, even in case of transient noises (man-made or natural) orders of magnitude larger than average perturbations without losing lock or even need to flag off data.
2. The rms motion of the mirror's mass, $\leq 10^{-8}$ m, is concentrated at very low frequencies (below 100mHz). Consequently, the residual velocity will be small enough for lock acquisition. Indeed the residual speed should be low enough that the main difficulty in lock acquisition is expected to come from a completely different direction, the photon pressure kick of the ramping stored light power.
3. Sufficient dynamic range (several mm) to guarantee indefinite interferometer lock without corrections made with sliding or rolling components.
4. All movements, obtained through purely flexural joints, actuated with electromagnetic field actuators. No noisy mechanical actuators are used after the initial tune-up.
5. No shear-stress joints and no reliance on friction whatsoever to avoid stick and slip internal noise generation.
6. High quality factor metals and low loss joints to best match the transition to the higher quality quartz suspensions.
7. Creep free materials in all components under stress.
8. Bakeability of the filters under load to reduce the residual creep to negligible levels. Other mechanical noise generating components, like for example electrical wiring, should be eliminated as well.
9. The suspended pendula modular geometry allows easy replacement of the lowest filters with possibly more advanced units.
10. Units narrow enough to be mounted offset in the BSC chambers for off-axis optics suspension (for multiple interferometer operation).

11. Allow staggered assembly of two SAS in a single BSC, thus, requiring a smaller number of BSCs for multiple interferometer implementation.
12. All metal construction for UHV compatibility.

In the SAS chain all seismic noise suppression in the frequency band of interest is obtained by purely passive methods, both for simplicity and reliability and to avoid up-conversions and accidental noise injection.

The residual r.m.s. motion, concentrated at the seismic attenuation resonances, is depressed by introducing a passive Ultra Low Frequency (ULF) pre-attenuator stage (a 10-30 mHz inverted pendulum and an similarly slow vertical movement filter) at the head of the chain to reduce seismic excitation of modes and by draining the remaining energy from the chain resonances by means of an active inertial damping system. The inertial damping system is capable to deal with the different body chain resonances. The active system can also boost the passive pre-attenuator's performance by means of some degree of low frequency active seismic isolation. The residual motion of the payload is reduced to a level low enough to be easily absorbed by the effective dynamic range of the mirror control actuators.

All active action is limited to 3-4 Hz, one third of the lower end of the frequency band of interest (10 Hz) to avoid re-introduction of the up-conversion noise generated by sensor's, actuator's and f.b. loop's non linearities.

Any f.b. loop noise is eliminated by the passive section of the chain which is measured to be quite linear and has negligible up-conversion levels.

In case of bothersome modes, invisible to the pre-attenuator accelerometers and hence impossible to be damped from it, a simple Eddy current magnetic damper suspended on an hexawire structure from F0 and acting on the first passive filter would be used. This would come at the cost of reducing the $1/f^n$ attenuation properties of the chain to a $1/f^{n-1}$ characteristic. This attenuation loss can easily be afforded by the large attenuation overkill of SAS. The passive Eddy current damper has the particularity of being most efficient for the chain modes with higher frequency that, because of the attenuation roll off, may hide below the accelerometer sensitivity level.

The SAS attenuation power would drive the seismic noise below the mirror and suspension thermal noise starting at frequencies above 4 Hz. Note that the SAS would be already in high attenuation mode at the 5 Hz noise peak occasionally present at the Livingstone site. The suspension control strategy is the triple pendulum one, based on a hierarchy of actuation authority, reacting from recoil masses, starting from the test mass going upwards. Each actuator must absorb the residual motion integrated over the reaction time of the actuator above. After this time the actuator in question is relieved from its load. The triple filter top element is actuated reacting against the inertial and static stiffness of the bottom passive filter that carries a lower platform. This platform, in its turn, is equipped with the triple pendulum external drive coils.

As the preceding stages these magnets have to hold the triple pendulum in the intended position only for the reaction time of the pre-attenuator actuators. This reaction time is characterized by the period of the slowest mechanical resonance, i.e. a few tens of seconds.

Given the small required efforts and the small time lengths involved, the available stiffness of the bottom filter is more than sufficient.

The pre-attenuator actuators in their turn are relieved of their average daily load by means of external pier actuators or more silent motorized springs (this action would be taken very seldom, in conjunction with independent lock interruptions).

The pre-attenuator movements can relieve the DC triple pendulum actuator required efforts in all degrees of freedom except the pitch and roll which, statically, are not reachable from the IP. In these directions the job would be made by (remotely) moveable masses changing the triple pendulum top common element equilibrium tilt angle. Impulsively the tilt recoil stiffness of the last filter is large. In DC it can be made arbitrarily large by simply playing on its suspension point height.

The above described alignment and control strategy is considered particularly attractive because it minimizes the required dynamic range of the mirror actuators, the in vacuum power dissipation and, in cases of power failure, the system settles at its average daily working point.

The biggest advantage of working with low frequency systems is their softness. Apart from large passive attenuation factors, softness allows large movement in response to small applied forces and low power consumption. At equal excursion the required standing coil power is proportional to the fourth power of the resonant frequency. A low stiffness is also intrinsically much safer; in case of accidental misfiring the actuators does not have the physical power to cause damage to the system. (An actuator capable to move a stiff system for a given distance, at end stop will have imparted to the system much more kinetic energy than an equivalent softer system. The imparted energies will differ by a factor equal to the square of the ratio of natural frequencies which, for a 3 Hz system will be 10,000 times more than for a 30 mHz one.)

It has to be noted that the movement softness, achieved with the inverted pendulum technique and with the geometric anti springs, is not obtained at the cost of higher material stresses. The cantilever blades are shaped in such a way as to maintain the desired stress level, independently from the working frequency. Non geometrical anti springs cantilever blades subject to equal loads are subject to similar stress levels as for example in the triple pendulum. High blade stress levels can be used to maximize already satisfactory attenuation performances by minimizing the amount of blade mass.

At equal stress levels and required performance, the use of cantilever blades, as opposed to helical blades, has the advantage of minimizing the spring mass, maximizing the spring internal resonant frequencies and avoiding mixing of linear with torsional motions.

Very importantly the blade springs lend themselves to much better assembly geometries, virtually eliminating the slip and stick noise typical of most helical coil seatings. This feature is deemed crucial for the elimination of this source of non gaussian noise.

2 Implementation

The proposed inverted pendulum, GAS filter configuration allows the present LIGO II requirements to be easily met while fitting into the existing vacuum envelopes and the LASTI testbed. The SAS performance can be further increased by adding a simple extension pipe between the BSC and its cap and adding passive filters to the chain. This addition, as a bonus, allows faster installation times and even the implementation of 2-in-1 seismic attenuation systems.

While a short version that fits in the existing vacuum vessels is studied, the most interesting design is that of a self-contained SAS system pre-assembled in a BSC vertical extension pipe for rapid (3 days) installation or replacement. This unique characteristic will substantially reduce the interferometer down times. The rapid installation scheme is more laborious with the shorter tower option but still feasible.

It is assumed in this report that the payload of the SAS will be a fundamentally unmodified GEO-like triple pendulum or an equivalent, optimized, 250kg system. The tall chain version allows the use of stretched triple pendula for better low frequency thermal noise performance. Upgrades to larger payloads are easily achievable.

3 Basic Design Concepts for the SAS

The proposed SAS chain is shown in figure 1.

The horizontal isolation is achieved by an Inverted Pendulum (IP) followed by a chain of simple hanging pendula.

The vertical isolation is achieved by a chain of Geometrical Anti-Spring (GAS) filters.

The IP and the first GAS filter are tuned at Ultra Low Frequencies (ULF) to attenuate the micro seismic peak and reduce residual rms motion. The other GAS filters are tuned between 0.3Hz and 0.5Hz to slightly exceed the frequency performance of the pendulum attenuation properties of the filters in the x and y directions. Angular frequencies are tuned at even lower frequencies.

Cross-coupling considerations require that all degree of freedom (dof) be attenuated progressively and uniformly. This is done well by the multiple stages of the SAS chain. We typically assume 1% of cross coupling between the vertical and horizontal motion for each stage, which is an easy requirement for the SAS mechanical construction.

Low-frequency rms motion is suppressed by active damping, using sensors and actuators only at the top of the IP. Any in-band noise, generated by the damping loop, is safely filtered out by the following passive filters.

Low frequency, viscous resonance damping can be achieved with simple feed back (f.b.) on Linear Variable Differential Transducers (LVDTs). Real active seismic attenuation and damping of higher level resonances require real accelerometers for inertial damping and more

complex feedback loops. These loops are already routinely operating in 3 dof Multiple In Multiple Out (MIMO) loops in the Virgo test facility with gain up to 1,000 and compensation notches for all the SAS internal relevant resonances. The Virgo test facility is a complete SAS chain including test and recoil masses.

The IP geometry, stiff in the vertical, pitch and roll degrees of freedom, effectively decouples the horizontal dof from the vertical ones. This simplifies the active damping design by dividing 6 dof loops into 3 dof ones. This geometrical advantage allows much easier and effective MIMO operation. Virgo has encountered much difficulty in stabilizing MIMO systems when horizontal and vertical dof were allowed to mix. No problem was encountered with the IP geometry and divided dof planes. The vertical dof is handled separately but in a conceptually similar way by Filter0 (F0), the first GAS filter, and its vertical accelerometer and actuator.

The IP provides a large actuation dynamic range for yaw and horizontal motion and requires only very small forces. Similarly, F0 provides large actuation dynamic range in the vertical direction.

Thanks to the softness, due to the ULF tuning, of the IP and Filter0, position adjustments of several mm are possible with low power voice coil actuators at the cost of few mW/mm (reference [1] to [3])¹. No mechanical position actuators are necessary in operation except for soft correcting springs that may be used only in initial tuning.

In case that some of the body modes had a node on the IP suspension point and turned out to be both uncontrollable by the inertial damping and bothersome, it would be treated separately. An optional disk, carrying magnets, suspended by a hexa-wire structure from F0 (see figure 2) would generate Eddy currents on the first passive filter thus damping even these modes.

An optional triplet of ULF GAS filters (figure 1) is considered to support the IP base to control the seismic tilt activity and enhance the IP accelerometer performance. This feature may prove to be unnecessary. It is considered to enable effective high gain feedbacks for ultra low residual rms motion of the payload. The filter triplet is not part of the baseline design and if proven unnecessary may be suppressed altogether. This compact configuration though may come useful in equipping the HAM chambers for bench support.

3.1 The Tall SAS Design

The typical SAS chain geometry is shown in figure 1; it is illustrated starting from the ground and ending on the test mass. Sensors and actuators are not shown for simplicity.

¹In the first installation some of the installation time savings will be eaten away by the necessity of taking out the existing SAS's hardware.

The standard (tall) SAS chain sits on a triplet of GAS filters supporting and balancing the IP base ring. The base ring is provided with twin tilt meters and a vertical accelerometer as well as LVDTs. It represents a 3 dof (vertical and tilt) platform and is acted on by 3 voice coils and 3 soft, motorized vertical springs (not shown, a pair of moveable permanent magnets, mounted on the reference structure, sandwiching and repelling a third small magnet mounted on the IP platform). These springs are used to tune the IP verticality and change its working point height. The three voice coil actuators, mounted coaxially to the 3 base filters, are slaved in MIMO mode to the 3 accelerometers, also not shown, to provide DC to 10 Hz tilt control and vertical pre-isolation. Below 5-10 mHz the voice coil drive signal is provided by the IP LVDT position sensors. Over 10 mHz the accelerometer signal is blended in. The triplet platform can initially be frozen out of function by tight LVDT-to-actuator feedback taking advantage only of its static positioning capabilities.

The next component of the SAS chain is the IP. The IP geometry is chosen as a primary horizontal filter because it can easily be tuned to Ultra Low Frequency (ULF), typically 15-30 mHz and it allows to gain height for the suspended pendula. It has an extremely good attenuation performance (figure 3). The suppression of the 9 Hz resonance in figure 3 (it is pushed at 40 Hz or above in the LIGO design) and the use of appropriate leg counterweights will further improve the IP performance and ease the active inertial damping FB loop design.

The IP top platform is provided, in a pinwheel configuration, with 3 horizontal accelerometers, 3 LVDTs, 3 voice coils and 3 motorized springs. LVDTs, voice coils and springs measure or act from the reference structure. The voice coils mounted roughly coaxial with the horizontal accelerometers and LVDTs are the instruments for the dynamic controls. The voice coils are slaved to the horizontal accelerometers through a MIMO DSP system. They provide damping of the IP and SAS chain horizontal/tilt recoil resonances. The DC dynamic range of the IP is ± 10 mm horizontally and ± 5 mm vertically. The coaxiality of the actuators and sensors will the MIMO matrices mostly diagonal, almost SISO-like.

The next component of the SAS chain is F0 the vertical-motion GAS filter mounted on the IP top platform.

The top filter is a ULF GAS filter (F0) whose central equipage is equipped with a vertical accelerometer, an LVDT, and a voice coil. The coil is slaved to the accelerometer above 10mHz and to the LVDT below. This GAS filter needs not being equipped with motorized tune springs because its vertical working point can be tuned acting on the IP base (a motorized spring will be needed if the triplet is suppressed). F0 is tuned below 100mHz. Similarly to the IP case, the vertical accelerometer feedback chills all vertical SAS body resonances.

Hanging down from the top filter is a chain of 3 or 4 passive filters (figure 4). The attenuation performance of the passive chain is purely based on the pendulum transfer function characteristics on all 6 dof, that is using the $1/f^2$ transmissibility starting from the relevant resonant frequency.

The Eddy current damper shown in figure 2 can be inserted between F0 and the first passive filter if needed.

The pendulum lengths, about a meter each determine the horizontal frequencies, yielding 0.5Hz resonances. The GAS filter vertical resonances are tuned between 300mHz to 400mHz (reference [4] and [5]) to exceed the horizontal attenuation performance. All angular resonant frequencies are even lower. The technical difficulty is all in the vertical motion filter because of the gravity pull. The vertical filters are achieved by means of mechanical systems. The load is supported over highly stressed cantilever springs. The vertical resonant frequency (naturally well above the Hz) is lowered by means of antisprings, magnetic in the case of Virgo (Reference [5]), geometric in the proposed system (reference [4]). The GAS filters are much simpler (figure 4 and figure 5), more stable and cheaper than the Magnetic Anti Springs (MAS) filters and yield better attenuation performance (figure ??). Additionally, they are designed for better creep and stick-and-slip performances. The measured GAS filter performance closely matched the simulated one thus validating the simulation and its completeness for the more complex description of the entire chain.

The tricky point in the design of a vertical filter is in controlling its internal resonances. The passive filter bodies have been built and tested to be resonance-free up to 250 Hz. The cantilever springs have internal resonances starting above 50 Hz (depending on blade thickness), all resonances below 100 Hz will be damped using inertial viscous dampers that preserve the full quality factor of the main mode, the technique proved very successful in Virgo. More advanced and simpler Eddy current dampers may be used in LIGO. Additionally, in LIGO all blade resonances will be staggered, filter-to-filter, using blades of different thickness in different filters. All possible noise paths will thus be interrupted. High frequency resonances are ineffectual because their peaks always remain well below the mirror thermal noise level; it will be checked to make sure that they will not accidentally pile up. The modal cross couplings that may generate noise paths, short circuiting the attenuation progression, are being checked as well.

The overall performance of several filters cannot be tested directly without an interferometric system because of the lack of sufficiently sensitive accelerometers. Currently, the performance of multiple (more than 2) attenuation units can only be simulated. It has been tested that the attenuation of two chained filters matches exactly, the convoluted performance of the two individual filters (reference [6]) and figure 7. It also matches well the corresponding simulation figure 8 (measurement taken on the setup of figure 9). Projected SAS chain performances are shown after the short SAS chain description. The simulation is obtained convoluting IP, pendula and GAS filter performances with a measured site noise spectrum. This convolution is still a simple minded one. A more evolved simulation with all six dof and including cross couplings, thermal noise, and control issues will soon be available within the LIGO end-to-end simulation model. Cross couplings are expected to introduce only small changes above 2Hz. Below 2 Hz some energy may leak from the horizontal to the vertical mode because of the faster vertical transfer function profile. The measurements of

figure 7 illustrate the mall amount of actual cross coupling. This is due to the fact that in the SAS chains attenuation is performed progressively and consistently in all stages. Note the wiggles at 0.6 Hz on the single filter measurement and at 0.5 Hz on the double filter one. They are due to the 2 filters tilt modes and are obviously only weakly excited. This despite the fact that the filters, initially factory aligned, had been intentionally mis-aligned and then simply re-aligned by mark one eyeballs (probably within a millimeter). This measurement illustrates the large assembly tolerances acceptable by the progressive passive attenuation scheme. Well aligned filters will present even less cross couplings.

The SAS chain will support either the triple pendulum directly or an optical bench holding different optical components.

In the case of an optical bench the SAS can be beefed up by the addition of more blades per filter and/or using stiffer ones to support the excess weight.

3.1.1 Rigid body mode damping in SAS

Rigid body modes of the chain may cause large payload residual rms motion if not properly damped. They will be detected and damped via sensors and actuators at the top of the chain taking advantage of the fact that all passive filters are connected in series to the F0/IP platform. The chain forms collective modes, which recoil against the F0/IP and are visible on their accelerometers. The energy of these modes is then easily drained by the feedback. The main tilt modes of the filters are naturally and sufficiently coupled to the horizontal modes to be visible and chillable by the horizontal accelerometers (Reference [7]). Some modes may have nodes at the IP and be invisible. The optional Eddy current damper disk will solve the problem if necessary.

3.2 The Short SAS Design

The proposed SAS chain requires the addition of a section of vacuum tube to vertically extend the BSC. It may be of interest to consider a system that fits inside the existing BSC vacuum vessel.

The shortened SAS of figure 2 still satisfies present LIGO2 requirements although with less safety margins and leaves less room for future improvements. It also has less horizontal and angular dynamic range and must rely on the BSC pier actuators.

The most important practical disadvantage of staying inside the existing vacuum vessel is that this SAS will be more difficult to assemble over the existing or modified cross tubes and this may entail somewhat longer installation down times.

The short SAS is a marginally cheaper solution because it has a smaller number of units but qualitatively the same ingredients are used. Consequently, it is not much simpler than the tall SAS, and it may require a larger attenuation share from the active system to compensate for the missing units.

The short SAS also leaves less openings for future upgrades. In particular, the tall SAS allows the use of longer triple pendula for better thermal noise performance (reference [9]).

Advantages and Disadvantages of the Short and Tall SAS

	Advantages	Disadvantages
<i>Tall SAS</i>	Better performance. Shortest Installation time. Can be interleaved (2-in-1).	Need vacuum extension. More expensive construction.
<i>Short SAS</i>	Fits existing envelop. Less expensive construction. Attaches to cross tubes.	Less overkill performance. Some longer installation time.

4 Performances Simulations of the SAS

The two simulated SAS chains comprise an inverted pendulum, a sequence of GAS filters connected by wires, which supports a modified version of the GEO triple pendulum.

The proposed modification consists on the implementation in the first GEO stage, of blades mounted in the GAS configuration, to improve the vertical attenuation as suggested in reference [15]. Additionally the top element of the triple pendulum would be acted on from the last filter structure.

No study has been done yet to investigate the mechanical cross coupling between the dof in the GEO suspension and the rest of the system. This coupling is expected to be small because the GEO triple pendulum is a balanced recoil system.

The simulation of both long and short SAS chains has been performed for the vertical and the horizontal dof independently.

The angular dof (yaw, pitch and roll) have not been investigated for the following reasons:

- 1) The very soft restoring torque of the wire gives yaw modes with resonance in the 10mHz region. The transfer function is expected to give a much better attenuation than the horizontal and the vertical case.
- 2) Similarly, one can tune the pitch and roll mode frequencies of the filters to obtain performances exceeding those of the other degrees of freedoms.

The transfer function and interferometer sensitivity curves have been obtained considering a simple model of the chain, with the following assumptions:

1. Unidimensional model.
2. All Internal modes are supposed to be above 50Hz and they do not degrade significantly the performances below 10Hz. Measurements of blade modes confirm this assumption for GAS filters while the filter body resonances are much higher.

3. The Inverted pendulum transfer function flattens above 10Hz. The first internal mode of the legs is expected to be around 40Hz in the LIGO design.
4. No cross coupling between the horizontal and vertical degree of freedom is considered
5. The suspension points of each pendulum are coincident with the center of mass of each GAS filter.
6. No wire tension has been considered.

The list of the parameters used in the simulation are shown in the following table

Table 1			
Short chain / Long chain			
	Length (mm)	Hor. Freq. (mHz)	Vert. Freq. (mHz)
Triplet	n.a.	High	n.a./100
IP	1468 / 3148	30/30	High
F0	n.a.	high	100/300
F1	650/1100	750/500	300/300
F2	650/1100	750/500	300/300
F3	n.a./1100	n.a./500	n.a./300
TP0	650/1100	750/500	300/300
TP1	300/300	900/900	2000/2000
TP2	300/300	900/900	high
Mirror	300/300	900/900	high

The vertical transfer functions corresponding to the two SAS options listed in table 1 are shown in figure 10. The horizontal transfer function is shown in figure 11.

The estimated horizontal seismic noise for both chains on the horizontal dof, (using the Hanford site measured seismic noise) is shown in figure 12. Note the higher frequency of the kick-in of the horizontal attenuation due to the higher frequencies of the pendula with respect to the GAS filters.

The figure 13 shows the cross over point between the seismic and the thermal noise. It illustrates how both SAS chains satisfy the requirement at 10Hz of exposing the pendulum thermal noise of a 300mm long quartz ribbon in the triple pendulum. Even the better thermal noise performance of longer quartz ribbon would be matched by the SAS attenuation capabilities.

Spectral seismic noise density with and without damping and for short and long SAS chains are shown in figure 14 and figure 15 respectively.

The integrated rms residual motion, an indication of the required mirror control dynamic range, is shown in figure 16 and figure 17 with and without a simple active inertial damping of the resonances. A better performance could be achieved with a higher gain.

5 Local controls

Local control of the suspension will be concentrated in two places: on F0 above the passive GAS filters chain and below, on the triple pendulum. The local control at F0 will have small bandwidth and large dynamic range. It will be responsible both for quieting all rigid body modes of the filter chain and providing local position control during data collection.

Local control at the triple pendulum is applied from recoil masses and it is assumed to be mostly decoupled from that at the top of the filter chain. Direct control on the mirror will be used only for lock acquisition. We expect it will be mostly shut off during observations, in part to avoid coupling ground motion and short circuiting the SAS, and in part due to the lack of sufficiently quiet and not perturbative sensors and actuators. The final aim would be to leave only a photon drive working on the mirror during data acquisition. The control authority of the other stages of the triple pendulum should be more than enough to deal with the small SAS residual motion. The actuator/sensor configuration is presently assumed to be essentially the one presently used by GEO. The triple pendulum top element is controlled, marionetta-like, by coils mounted from the last passive filter.

The triple pendulum is actuated from local recoil masses of different kind. Their recoil may perturb SAS and re-excite its modes. All action on the triple pendulum actuators can be used as a feed forward added to the IP inertial damping. The inertial damping will then critically damp any re-injected energy from the triple pendulum actuators.

Only the controls at the top of the SAS chain are discussed in this report. They will be applied directly to the top GAS filter by means of voice coil actuators acting against the reference frame. Position sensing will be made by LVDTs on the top GAS filter (sensitivity $10^{-7}\text{m}/\sqrt{\text{Hz}}$ at 10mHz). The upper platform controls must have a global correction to for tidal motion, thermal drift, et cetera. The interferometer signal itself, or external sensors in the other directions, will provide this correction. The LVDT and accelerometer signals will dominate at low frequency and be blended with a 10mHz crossover. The cross over frequency may be different in different dof.

A bandwidth of 5Hz is judged sufficient to control and chill all rigid body modes of the filter chain; this will be tested at Caltech in the near future. Tests are also underway at Virgo for a similar filter chain (figure 18). In the Pisa tests the control system is quite advanced, the limiting factor may be given by mechanical shortcomings (internal resonances of the IP).

All working points, except pitch, will be positioned by the IP/F0 slow positioning minimizing the DC component of the corresponding IP/F0 forcers. A counterweight based pitch control will be needed at the top mass of the triple pendulum with a range determined by the engineering tolerances and a finesse smaller than the triple pendulum AC control range. Achievable tilt control range of the triple pendulum needs to be determined. This counterweight will be mechanically tuned during installation. It may be necessary, for reasons of limited AC pitch control and/or for the desire to null the global pitch after evacuation and

baking, to have a remotely controlled fine pitch adjustment on the top mass. The ability to apply this nulling after the first lock acquisitions would be quite helpful, and some possible techniques are being evaluated.

It has been said that the ULF filtering action and active damping of the IP/F0 system are limited to 4 d.o.f. (vertical, 2 horizontal and yaw) while the filters additionally show the 2 tilt modes.

These tilt modes may at first sight seem uncontrolled. In a filter chain though the simple modes of individual filters do not exist anymore because they have merged into an equal number of chain modes in which tilt and horizontal modes mix, as clearly illustrated for example in figure 9-b of Ruggi's report, reference [7] (the coupling to the vertical and torsional modes of the chain is strongly reduced by symmetry reasons, as observed by Ruggi).

Consequently the filters contribute to the chain with four tilt-horizontal modes each at separate frequencies.

The horizontal component of these modes can be picked and chilled by the accelerometers of the IP as in the high-gain, multiple-notch feed-back scheme demonstrated by the Virgo IP operation and shown in figure 18.

Virtually all horizontal modes, calculated and measured by Ruggi appear in the IP accelerometer signal.

A perceived danger is that some of these modes may have a node at the IP location and be effectively uncontrollable by the inertial damping system. (Note that this is not a property of a 4 dof control, in line of principle, even with a fully 6 d.o.f. controlled head of chain, there may exist chain modes that have a node at the suspension point and therefore cannot be controlled.)

These modes, being unreachable by the inertial damping system, would also not be reached and excited by the seism and in principle could be ignored. If these hidden modes proved to be a problem (for example if they were excited by the mirror control actuators) they can be neutralized easily. This would be done by noting first that, if a mode has a node at the IP level, for momentum conservation reasons it cannot have another node also on the next (first) filter. To act on these, hidden, modes, a rigid disk would be mounted hanging on hexawires from F0. It would carry a ring of magnets acting on OFHC copper plates bolted on the top surface of the first filter.

The viscous damping introduced would effectively reduce the $1/f^{2n}$ filtering action of the chain to $1/f^{2n-1}$, but this can easily be afforded by the large SAS attenuation reserve. The possible e.m. coupling of the magnets to outside magnetic fields can be minimised by using U-shaped dipoles to confine the return field and would anyhow be of little concern this high on the attenuation chain.

5.1 Accelerometers

The inertial damping feed back is based on Virgo type accelerometers, i.e. a mass free to move in one direction, sensed by an LVDT and kept at the null point of the LVDT by a forcer operated in the feed back loop. The forcer drive current is proportional to the sensed

acceleration.

The choice of the null point accelerometer instead of the more classic seismometers or geophones was dictated by the better linearity of the null point instrument. The concern was that accelerometer non-linearities would have triggered upconversions in the feed back loop. These upconversions would probably have been acceptable because of the large passive attenuation offered by SAS but it was deemed wiser to eliminate them at the source.

5.1.1 Advanced Accelerometers

The SAS payload rms motion is mainly generated by the chain body resonances excited by seismic activity. To reduce it to the desired level, sensing of and reacting to the chain's modal recoil of the F0/IP platform is used to chill the body resonance excitations. As a consequence the rms at the payload support point (or at the mirror) can be considered proportional to the sensitivity of the f.b. loop and eventually of the accelerometers.

The SAS chains can operate under simple velocity damping of its resonances. This already depresses the residual rms noise down to 410^{-8} as shown in figure 16 and figure 17. Commercial accelerometers or of design directly derived from the Virgo accelerometers are sufficiently sensitive (and sufficiently insensitive to the orthogonal directions) for this task (the Virgo homemade accelerometers are built and tested for low transversal sensitivity and UHV compatibility).

At Virgo the IP is already routinely operated on 3 dof MIMO feedback with a peak gain of 1000 and unity gain limits at 10mHz and 4Hz (figure 18). At low frequency, the accelerometer sensitivity is blended with the LVDT sensitivity to provide DC control. Higher loop gain and more sensitive accelerometers would further dig into the residual rms motion. This may not be practical in Virgo because the horizontal accelerometer, being partially sensitive ($10^{-2} - 10^{-3}$) to vertical noise, would couple this noise into the horizontal plane through the feedback loop. When the product of the gain times the unwanted vertical sensitivity becomes bigger than 1, further increase of gain only worsens the overall attenuation performance. The proposed SAS chain is predisposed to go beyond this obstacle.

Advanced accelerometers with hundred times improved sensitivity are under development (reference [8]) to allow true active seismic pre-attenuation in front of the passive chains. Care is being taken to make them less sensitive to transversal acceleration. Despite this, they would still be hampered by the vertical seismic noise. The filter triplet supporting the IP will make the accelerometer full potential available on the IP platform controls thanks to the vertical pre-attenuation they provide. Similarly to F0 the triplet will be made of ULF GAS filters and equipped with sensors and actuators.

The triplet will provide positioning in tilt and the vertical direction on top of the tilt seismic noise filtering to improve the IP performance.

Although this technique has not been tested yet, the triplet is based on tested components and it is not a critical item. The triplet can easily be electronically frozen out by a tight loop

between the LVDT and the actuator to be thawed only when a working control scheme is developed. Consequently, although the TRL of this component is lower it is not a worrisome item.

Similarly the vertical accelerometer at the top of F0 operates in the IP horizontally quiet environment. An advanced vertical accelerometer can be operated with full profit in this direction without further modifications.

Advanced accelerometer operation may reduce rms residual motion enough to enable low-noise photon mirror drives instead of the electrostatic or electromagnetic drives presently foreseen for the mirror controls.

6 Vacuum Compatibility

The SAS is a fully metallic and ceramic system.

The electrical wiring will be isolated with kapton or equivalently UHV compatible resin and will be baked over 200°C.

The motorized springs will be actuated by UHV stepping motors. Full bakeability and UHV compatibility has been measured in Virgo for motor of at least one manufacturer. All electronics will be built in ceramic hybrid technology to preserve bakeability and full UHV compatibility.

The entire fully-assembled and loaded SAS chain will be pre-baked at 150°C (200°C for all organic components) for a week under vacuum or neutral and/or oxidizing atmosphere. After baking the SAS will be stored in neutral atmosphere until installation. Clean assembly is compatible with existing on site procedures and tooling with minimal changes of existing clean rooms. The SAS should also be re-baked in situ and under vacuum at lower temperature, the highest tolerated by the mirror and quartz suspensions.

In the SAS design there are no independently or differentially pumped volumes and absolutely no enclosed volumes that could trap and leak gases (let alone increasing complexity and costs).

7 Creep, Creak, and Sag

The structure of the S.A. chain is carefully engineered not to exceed, at any point, the certified safe material stress levels for micro creep (reference [10] and [11]).

Stress levels of 60% of the yield point in maraging have already been certified. The GAS filters of present design are stressed at the same level of the triple pendulum blades. Higher stresses may be used in the GAS filters (and in the triple pendulum) to further improve

their performances (see figure 19) after proper stress level certification is obtained. A creep testing facility is being built for this purpose (figure 20).

The pre-baking under stress has been observed to completely exhaust the creep of the available dislocations (reference [11] and [12]). This treatment has reduced the observed creep rate below 10^{-12} m/day, it should reduce acoustic emission less than 1 event/day and overall sagging well below the micron per year.

Pre-baking essentially ages the suspensions for an equivalent time of more than 1000 years.

The time between mechanical failures after this process can be estimated of the same order of magnitude.

To eliminate creak and stick and slip, another source of non gaussian noise, all mechanical joint surfaces have been replaced with zero-shear joints, see inserts in figure 4, in which the stress is perpendicular to the contact surfaces. Additionally all the contact surfaces will be covered with a thin layer of indium alloy that will flow during baking and effectively weld the chain into a monolithic structure (reference [13]).

All movements (except very rare one obtained with pier movements) are achieved acting on flexural joints with analog voice coil forcers (that produce no vibrations) or with stepping motor-actuated soft springs that generate very little vibration noise.

7.1 Thermal stability

Estimation of the amount of drift in the vertical mirror position associated to thermal effects on the IP and on the filter cantilever blades. Thermal effect on the drift of the horizontal IP position observed at VIRGO.

7.1.1 vertical drift

We have performed the calculation for two different lengths of the IP legs (1.5 m and 3 m) and for two different materials (aluminum and steel). We assume that:

- the maximum predicted thermal variation is $T = \pm 2^\circ\text{C}$;
- the drooping of the blades's tip is $\Delta z = -40\mu\text{m}/^\circ\text{C}$
- the number of stages provided with blades is 5 in the short tower, 6 in the long one;
- the thermal expansion coefficients used are: $\alpha_{\text{Al}} = 2.4 \cdot 10^{-5}$, $\alpha_{\text{steel}} = 1.2 \cdot 10^{-5}$

With this numbers, the expected mirror vertical drift in the 4 cases is:

	short	long
<i>steel</i>	$-364\mu\text{m}$	$-408\mu\text{m}$
<i>aluminum</i>	$-328\mu\text{m}$	$-336\mu\text{m}$

7.1.2 horizontal drifts

Drifts in the horizontal position of the VIRGO IP (of the order of $100\mu\text{m}$) have been observed on the VIRGO IP in the 24 hours period. In the following we attempt a simple explanation of this effect. Let us assume that the IP base is tilted by an angle α . At the equilibrium the IP will then form an angle θ_0 with the vertical axis.

Given the stiffness k , the mass m , the length l , the following equilibrium equation holds (in the small angle approximation):

$$mg\theta_0 \approx kl(\theta_0 - \alpha) \quad (1)$$

The relative temperature variation with the temperature depends mostly on the Young modulus variation:

$$\frac{1}{k} \frac{dk}{dT} \approx \frac{1}{E} \frac{dE}{dT} \approx -10^{-3} K^{-1} \quad (2)$$

Due to the stiffness variation, the IP equilibrium position will change to a new angle θ_1 given by:

$$mg\theta_1 \approx k'l(\theta_1 - \alpha) \quad (3)$$

where

$$k' = k + \frac{dk}{dT} \Delta T \quad (4)$$

This effect turns into a horizontal drift

$$\Delta x = l(\theta_1 - \theta_0) \quad (5)$$

Using eqs. (1), (2) and (3) one gets:

$$mg(\theta_1 - \theta_0) = kl(\theta_1 - \theta_0) + l \frac{dk}{dT} \Delta T (\theta_1 - \alpha) \quad (6)$$

and

$$\alpha = \theta_1 \left(1 - \frac{mg}{k'l} \right) \quad (7)$$

Eq. (7) can be simplified. Using the expression for the IP resonant frequency and eq. (7):

$$\frac{mg}{k'l} \approx \frac{mg}{kl} \approx 1 - \frac{\omega_0^2 l}{g} \Rightarrow \alpha \approx \theta_1 \frac{\omega_0^2 l}{g} \ll \theta_1 \quad (8)$$

Using (8), eq. (6) can be written in the form:

$$(mg - kl) (\theta_1 - \theta_0) = l \frac{dk}{dT} \Delta T \frac{g\alpha}{\omega_0^2 l} \quad (9)$$

Therefore, the horizontal drift (5) can be calculated:

$$\Delta x = -\frac{g\alpha}{m\omega_0^4} \frac{dk}{dT} \Delta T \quad (10)$$

Assuming $m = 500$ kg, $\alpha = 1$ mrad, $\omega_0 = 2\pi$ (0.03 Hz) one gets:

$$\frac{\Delta x}{\Delta T} \approx 15 \text{ } \mu\text{m}/\text{K} \quad (11)$$

8 Flexibility Features

The S.A. chain presents a large load dynamic range, it can support a ton payload without modifications. It is advisable to put excess mass on the triple pendulum top so that different configurations with different weights can be loaded without even re-tuning the SAS chain. Additionally a heavy payload, compared with the F0 mass, increases the proportion of F0 recoil and favors the resonance chilling procedure for rms reduction.

The SAS structure, including the safety structure, fits inside a 2m diameter envelope while the BSC chambers present a 2.6 m inner diameter. This leaves the possibility to make eccentric assemblies up to 60 cm in radius to match offset beam position, figure 21. Vertical beam offsets are also easily taken care of by simply changing the suspension wire length.

8.1 Fast Installation Procedures

In the design of SAS, great care was taken to reduce the installation down time. Presently, 18 man-years spread over 9 months are necessary to mount the stack system. The tall IP SAS is designed for plug-in assembly on the BSC followed by a Snap-On mount of the mirror suspension stages.

The SAS is mounted inside a section of vacuum tube 2.6 m diameter, 2 m tall, fitting between the BSC chamber and its cap. The vacuum pipe is provided with brackets protruding downward to support the IP base ring and the SAS chain safety and reference structure.

The SAS is lab pre-assembled, pre-baked, tuned and tested with its mirror suspension system or with an equivalent dummy load.

Pre-baking, testing, and storing will require large space and high crane ceiling. These operations can be done in 4 locations:

- in the Caltech Synchrotron hall (starting in mid-2003 when the Minos experiment will vacate the premises)
- in end station 2 at Stanford

- in the staging halls of the 2 LIGO sites

After tuning, each element of the SAS chain is suitably immobilized against its earthquake restraint system into its safety structure, bagged, tilted horizontally, and shipped to the site. Transportation will be made by means of standard food-grade containers, which are aluminum lined to insure cleanliness.

Upon arrival at the site, the SAS is re-erected and plugged on its BSC chamber.

The safety structure, being built for earthquake containment, can easily support the 1 g accelerations typical of trucking on bad roads.

After placing the vacuum tube extension on the BSC chamber, the SAS chain is released, tuned for tilt corrections, and re-tested. The vacuum pipe section is then sealed with the BSC cap and is ready to be loaded with its mirror suspensions system. The retracted transport latches doubles up as earthquake restraints.

The procedure on site can be as long as three shifts per tower.

The short SAS, not having the advantage of the vacuum pipe extension to mount on, may be somewhat slower in assembly, but it still designed as a fast assembly, pre-tested and tuned unit.

Cleanliness can be maintained from the post-assembly bake to the in situ installation by means of sealable skirts and plastic caps that mate to the existing BSC movable clean rooms and BSC caps.

Before arrival of the new SAS, the old stacks must be removed, the piers actuators must be disconnected from the cross tubes, the cross tubes eliminated, and the bellows flanged out (or the cross tubes replaced for the short tower). The piers may be connected to the BSC for additional rigidity. The stack disassembly time may be the leading time constraint for the first installation of the SAS system. Further upgrades or modifications will take full advantage of the SAS plug-in technique and can be much faster.

The fact that SAS are made for horizontal transport, makes their safety/reference structure automatically resistant to more than 1 g of transversal forces. This feature already exceeds the earthquake requirements on the sites.

8.2 Earthquake safety

During the IP transfer function measurements at Virgo the IP base was routinely shaken, by means of computer controlled compressed air pistons, over excursions of several millimeters spanning all frequencies, up to several Hz. This was necessary to have a minimum of detectable signal on the accelerometers below. The chain took this abuse without problems. Earthquakes with small excursions should present no problem for either the SAS chain or its payload. Problems arise when the quake excursions exceed the safety end-stops. At this

point the attenuation properties of the chain are bypassed and the transmitted energy may shatter the SUS. There is no worry about dropping any filter even in case of broken suspension wire. The filters are safely caged in the safety structure. The safety structure itself can take several g acceleration.

8.3 Simplicity

Although the system seems complex at first sight, it is actually quite simply built, made of modular GAS springs and an IP. All movement in the stress path are obtained by means of flex joints, and the only moving parts, the motorized springs, are mounted on the vacuum vessel/safety structure completely outside the SAS chain and the stress path. Also, the maximum force applied with the springs tuning is of just a few Newton and the motorized sleds are never subject to significant load.

The GAS filter main resonance frequency are factory set, the entire chain is lab pre-tuned thus greatly simplifying their installation and use. The only foreseen tune-ups in situ will be the IP leveling in the tower (by means of the motorized springs or pier actuators), and the payload tuning. These operations will likely be automated. In any case the entire chain can be pre-wired before installation.

The SAS chains are expected to be controlled wireless (except, maybe, for the motorized springs, which would be pre-wired through the vacuum tube). This will also greatly contribute to simplify the installation procedure.

The fact that the tall SAS are pre-assembled in a separate lab and simply plugged-in in situ will greatly lessen the time pressure of open vacuum operations thus introducing an effective simplification of procedures.

8.4 The 2-in-1 option

The tall SAS chains are almost empty and can be intertwined. This opens the road to building 2-in-1 interferometers. To intertwine the chains the gas filters are staggered vertically and the IP legs are staggered 60° angularly while the IP base plate would be shared, figure 22 and figure 23.

The two SAS chains are completely independent and the two interferometers are then uncorrelated.

Any separation between 0 and 120 cm is achievable by simply choosing the twin tower orientation with respect with the beam.

In this configuration up to 3 interferometers could be installed in both sites without major changes to the vacuum system and large additional costs (see figure 24).

8.5 2-in-1 fast Implementation Scenario

The addition of a third interferometer would obviously be an option for the future.

A SAS interferometer would supposedly be already in operation. The interferometers could be rapidly unplugged and replaced by the 2-in-1 structure by simply exchanging extension pipes; the extracted, modular SAS hardware could be easily reconditioned and recycled in the 2-in-1 of the other site.

9 Wireless controls

Electrical wiring is an excellent candidate to introduce noise in the signal, both electrically and mechanically. While in the early stages of the SAS chain some excess noise from wiring could be tolerated because it will be filtered out by the passive chain components, at the triple pendulum interface level all cabling and other loose and plastic components may inject random slippage noise and should be eliminated. This should be done as early as possible on the chain. The solution involves the use of remote controls powered by solar cells illuminated by LEDs placed outside the vacuum. This technique, necessary in any advanced interferometer, still needs to be developed. No major obstacles are expected because all necessary components have been thoroughly studied for satellite operation. It may be implemented immediately in 2004 or together with the advanced mirror in 2007.

10 Testability

The building block prototypes (GAS filters) have already been built and are being tested and further improved, figure 5 and figure 9. By the end of 1999 we will have assembled a complete SAS preliminary design (see figure 25).

The first short prototype would be tested early on in LASTI. To allow the vacuum vessel closing, even in the low LASTI ceiling, it will be necessary to replace the present tall cap with a short ring and a short cap to be craned in successively. By the end of 2000, after air testing, disassembly and re-cleaning, the system will be ready for vacuum tests.

If the tall tower was chosen a new prototype would be necessary.

This prototype would be mounted in the place now occupied by the BSC and HAM prototypes at the Caltech Synchrotron.

The 2-in-1 concept could be used in TNI for thermal noise studies of different mirror suspension configurations using a single vacuum chamber. In this case the 2-in-1 prototype would be built at a later time. The TNI measurements would completely validate the SAS system including its active attenuation, control and alignment procedures.

The mirror suspensions of the day will be used in this system to form a 0.5m Fabry Perot interferometer.

Tests will include active SAS locking procedures and thermal noise studies.

- 1999 Prototyping of SAS components.
Dimensioning of SAS prototype system.

- 2000 Finalize SAS system design.
Develop controls.
Develop accelerometers.
Start short tower tests in LASTI.
Build 2-in-1 unit.
- 2001 In vacuum tests in LASTI
Break in control techniques in LASTI.
Operate the 2-in-1SAS units in air
Develop wireless actuators.

- 2002 Run 2-in-1 in vacuum thermal noise tests on F.P.
Finalize SAS construction design.
Develop fast installation procedures.
Start SAS construction.
Develop SAS fast assembly procedures.

- 2003 Constructions of all SAS units
(the Minos experiment clears the Synchrotron space in 2003)
Pre-assembly, baking, and testing of units in Synchrotron and/or EHN2 in Stanford.

- 2004 SAS installation and commissioning in situ

- 2005 Run thermal noise tests on F.P. configuration in TNI or LASTI
with 2007 mirror suspensions.

11 Technology Readiness Level

The TRL evaluation is probably not the proper way to evaluate a system like the seismic attenuation system, rather the probability to arrive (or risk not to) with a given solution in time for the 2004 installation or at least with a backup solution should be listed.

The proposed design is based on an existing Virgo design, which is presently being installed on the Virgo short interferometer. Therefore the proposed solution has a very good fall back solution and very low risk not to be ready in time. The Virgo system has a Technology Readiness Level (TRL) between 7.2 and 8. Several improvements over the Virgo design have been considered, designed and tested.

The proposed SAS scheme presents some improvements on the critical line that has TRL above 6.2. New components with lower TRL are not critical (can be dropped off loosing just

the improved performance but not losing the overall system functionality). They thus do not lower the overall SAS TRL rating.

Other options with lower TRL are considered, studied and developed but will not be integrated until they reach a sufficient TRL. The TRL breakdown is in the following table.

Safety Reference Structure	8
Structure with same geometry and soundness of equal field tested system.	
Demonstrated to be rigid enough as reference for actuators in a taller structure.	
Inverted Pendulum	
Scaled geometry from the Virgo Inverted Pendulum.	
Half way between the Virgo tall and short towers.	
IP actuators	
Maxwell Pairs coils and permanent magnets as in Virgo	8
Motorised springs	5.2
(2D voice coil, option)	2.0
IP Sensors	
LVDT built As in Virgo	8
Accelerometers	
Initially as in Virgo	8
(Mechanically improved and low thermal noise enhancement)	3.1)
Filter Zero	
Geometry based on the GAS technique to be tested for transfer function	
and to implement vibration damper, Virgo like or inertial eddy current damper	
Filter Mechanics	5.2
Virgo dampers	8.0
(Eddy Current Dampers)	3.1)
Actuators	
Voice Coil	8.0
Sensors	
LVDT	8.0
Accelerometer	8.0
Suspension Wires	
Based on completely tested double nail head wires and half cup retainers	
8.0	
Standard Filter	
Filter Mechanics	6.2
Virgo dampers	8.0
(Eddy Current Dampers)	3.1)

12 Costs

The production cost estimations for all mechanical components have been made based on actual prototype costs, actual bids, and cost estimations made by us or by the company that built Virgo extrapolating from the actual costs incurred in the construction of equivalent components built for the Virgo chains. Bids from U.S. firms will be obtained before presentation to an external committee.

	Cost (k\$)	Qty	Total (k\$)
Tri filter	25.5		
Inverted pendulum	26.6		
Filter zero	9.7		
Standard filter	8.9		
Support structure	15.0		
114" diameter 80" long vacuum pipe extension with standard LIGO flanges and 6 12" ports	25.5		
114" diameter hat with standard LIGO flange	11.1		
Accelerometer	3.5		
Actuation coils	1.0		
Tuning motors	2.0		
LVDTs	0.5		
	Cost (k\$)	Qty	Total (k\$)
Cost of single SAS chain			
Tri filter	25.5	1	25.5
Inverted pendulum	26.6	1	26.6
Filter zero	9.7	1	9.7
Standard filter	8.9	4	35.6
Support structure	15.0	1	15.0
114" diameter 80" long Vacuum pipe extension with standard LIGO flanges and 6 12" ports	25.5	1	25.5
Total excluding accelerometers, LVDTs, coils and motors			137.9

	Cost (k\$)	Qty	Total (k\$)
Cost of 2-in-1 SAS chain			
Tri filter	25.5	1	25.5
Inverted pendulum	26.6	2	53.2
Filter zero	9.7	2	19.4
Standard filter	8.9	8	71.2
Support structure	15.0	2	30.0
114" diameter 80" long Vacuum pipe extension With standard LIGO flanges and 6 12" ports	25.5	1	25.5
Total excluding accelerometers, LVDTs, coils and motors			224.8

	Cost (k\$)	Qty	Total (k\$)
Cost of Short SAS			
Inverted pendulum	26.6	1	26.6
Filter zero	9.7	1	9.7
Standard filter	8.9	2	17.8
Support structure	15.0	1	15.0
Total excluding accelerometers, LVDTs, coils and motors		79.8	

	Cost (k\$)	Qty	Total (k\$)
Six accelerometers	20.5		
six actuation coils	9.0		
six tuning motors	12.0		
six LVDTs	3.0		
Total active components per tower			44.5

All components are already made according to U.H.V. compatible designs, and use U.H.V. compatible materials even if not all the U.H.V. procedures have been applied to the prototypes so far. Suitable surface treatments may increase costs.

Competitive bidding and series production may bring costs further down.

Acknowledgments

We want to thank to GVNN for his support, criticism, and suggestions in writing this report.

References

- [1] R. DeSalvo, A. DiVirgilio, A. Errico, F. Guotong, I. Ferrante, et al: “Performance of an Ultralow Frequency Vertical Pre-isolator for the Virgo Seismic Attenuation Chains”, *Nuclear Instruments and Methods in Physics Research A* 420, 316, 1999.
- [2] G. Losurdo: “Ultra-low Frequency Inverted Pendulum for the Virgo Test Mass Suspension”, Scuola Normale Superiore di Pisa Classe di Scienze, 1998.
- [3] G. Losurdo, M. Bernardini, S. Braccini, C. Bradaschia, C. Casciano, et al: “An Inverted Pendulum Preisolator Stage for the Virgo suspension system”, *Review of Scientific Instruments*, 70, 2507, 1999.
- [4] A. Bertolini, G. Cella, R. DeSalvo, V. Sannibale: “Seismic Noise Filters, Vertical Resonance Frequency Reduction with Geometric Anti-Springs, a Feasibility Study”, *Nuclear Instruments and Methods in Physics Research A*, 00, 1999.
- [5] M. Beccaria, M. Bernardini, E. Bougleux, S. Braccini, C. Bradaschia, et al: “Extending the VIRGO Gravitational Wave Detection Band Down to a Few Hz: Metal Blade Springs and Magnetic Antisprings”, *Nuclear Instruments and Methods in Physics Research A*, 397, 1999.
- [6] F. Frasconi, et al., “Performance of the R&D Super-Attenuator (SA) Chain of the Virgo Experiment”, Rencontres de Moriond, January 1999
- [7] P. Ruggi, Virgo report: “Measurement of the Normal Modes of the First VIRGO Superattenuators”, Code: VIR-TRE-PIS-4600-151, Issue 2, February 24, 1999.
- [8] Alessandro Bertolini, “Low thermal noise accelerometers for active control of a very low frequency seismic isolator”, LIGO note to appear as LIGO T990077-00-D
- [9] Eric Black, “Thermal noise in coupled harmonic oscillators” LIGO technical note
- [10] M. Beccaria, M. Bernardini, S. Braccini, C. Bradaschia, G. Cagnoli, et al: “The Creep Problem in the VIRGO Suspensions: A Possible Solution Using Maraging Steel”, *Nuclear Instruments and Methods in Physics Research A*, 404, 455, 1998.
- [11] Riccardo deSalvo, “Non stochastic noise in gravitational wave detectors”, Second Gedoardo Amaldi conference on Gravitational waves, CERN CH 1-4 July 1997.
- [12] Vincenzo Rubino, “Studio del Microcreep nelle sospensioni degli specchi di Virgo” tesi di laurea, Universita’ di Pisa 1996/1997
- [13] R. DeSalvo, et al. “Design considerations for seismic attenuation systems in gravitational wave detectors”, Rencontres de Moriond, January 1999.
- [14] Reference from TAMA on magnetic damping.

- [15] K.A.Strain, "Isolation, control and design aspects of the adaptation of a GEO suspension design to LIGO" ,suspension summit released doc. May 5,1999
- [16] G. Losurdo, private communication, Pasadena August 1999

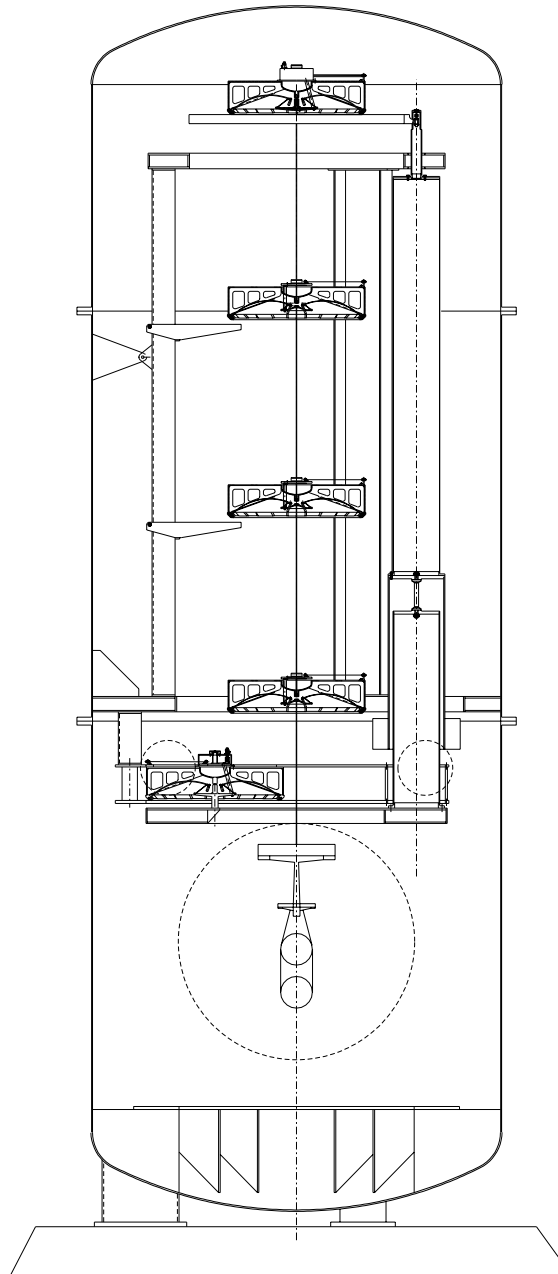


Figure 1: Tall SAS schematic view. The entire structure is assembled inside an extension pipe (blue) that mounts between the existing BSC chamber and its cap (black). The SAS itself is supported on a safety/reference structure (light blue) bolted to the extension pipe. The IP. (red) sits over a GAS filter triplet (light green) and supports the F0 (dark green). The filter triplet (optional), the IP and the F0 represent the active part of SAS. The 3 or 4 GAS filters (orange) hanging from F0 are the passive part of the SAS, they support the triple pendulum payload (yellow).

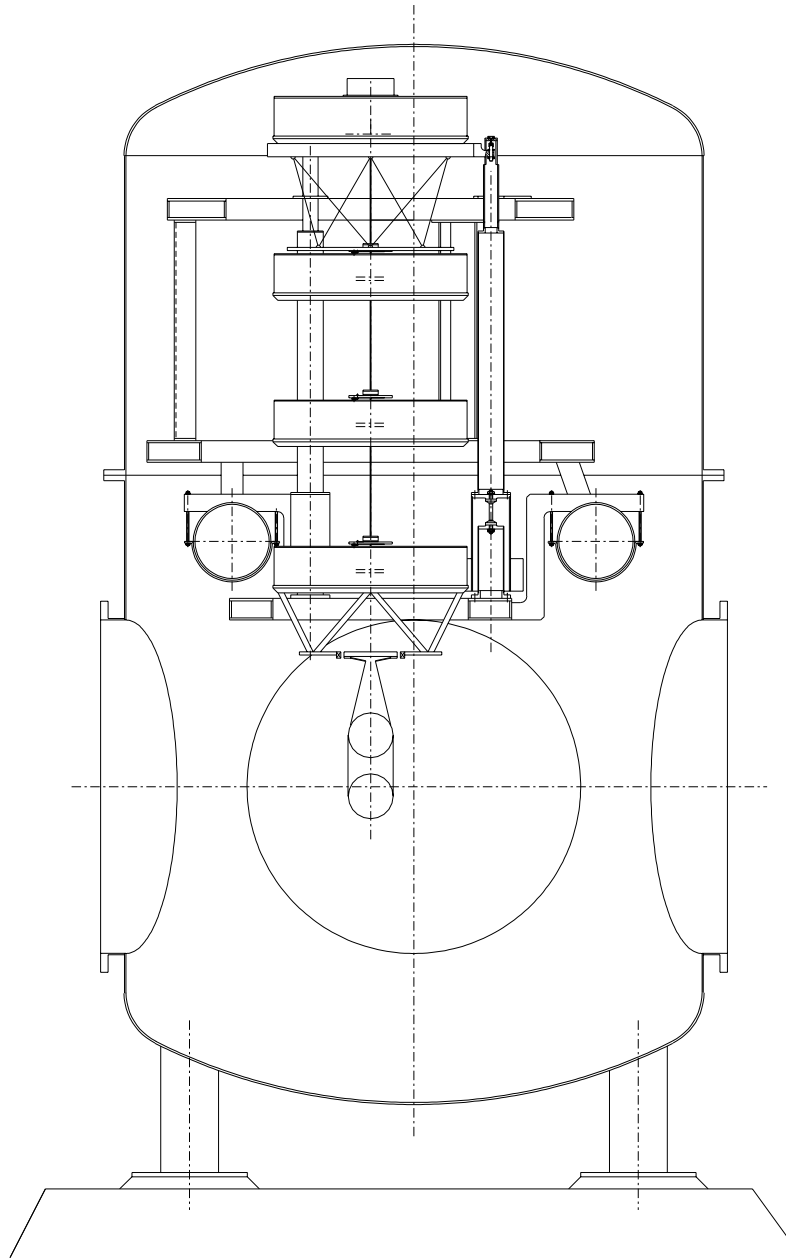


Figure 2: Short SAS schematic view. A shortened version of the SAS can fit in the existing BSC chamber. It is mounted over the existing cross tubes instead than on the extension pipe. Visible, hanging from F0 is a hexawire suspended disk. It would be loaded with magnets and provide eddy current chain mode damping. Filter 3 carries an octo-pod structure supporting the triple pendulum control coils.

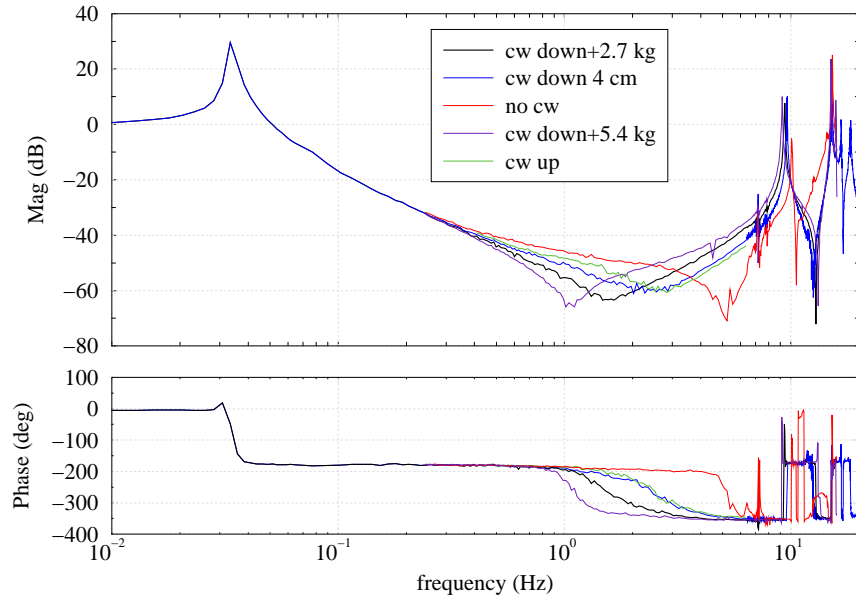


Figure 3: Performance of the Virgo inverted pendulum table. Mechanical transfer function of the 6 meter IP of the Virgo superattenuator on the horizontal dof. The 5 curves were measured with different configurations of counterweight to null the batting point effect. The large peak at 9 Hz is due to the main resonance of the IP legs. (Courtesy of the Pisa VIRGO Group). The LIGO prototype should not show any IP leg resonance below 40 Hz due to better design of the legs aspect ratio and because of the suppression of a heavy flange present at half length on the Virgo IP legs. An additional 10 dB may be gained between 1 to 10 Hz.

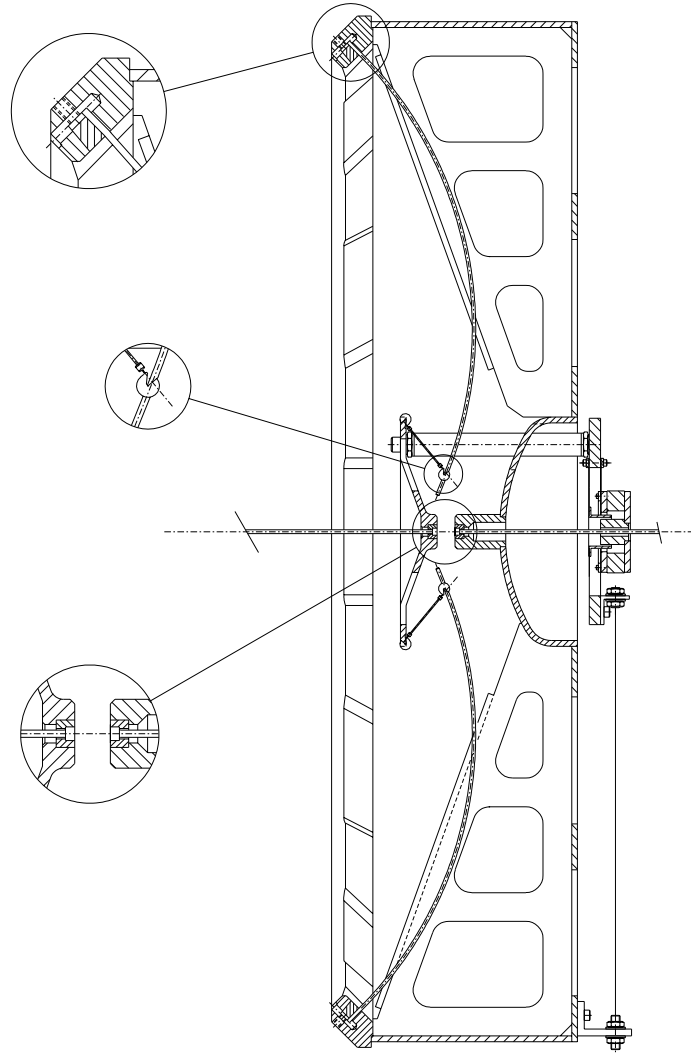


Figure 4: Standard Geometric AntiSpring Filter A rigid body (black) supports the stressed blades (red) hooked to a load disk (blue) through wire hooks (green). Suspension wires (orange) connect the filter to and from other filters in the chain. The wires are connected to the filter body by means of half cup inserts (violet in central blow-up insert) The blades are attached to the filter body by means of calibrated wedges (violet in left blow-up insert) and the blades tip are fastened to the hook wire (right blow-up insert) by means of hooks which contact surface is perpendicular to the stress direction. Three centering wires (yellow) constrain the load disk to a purely vertical motion

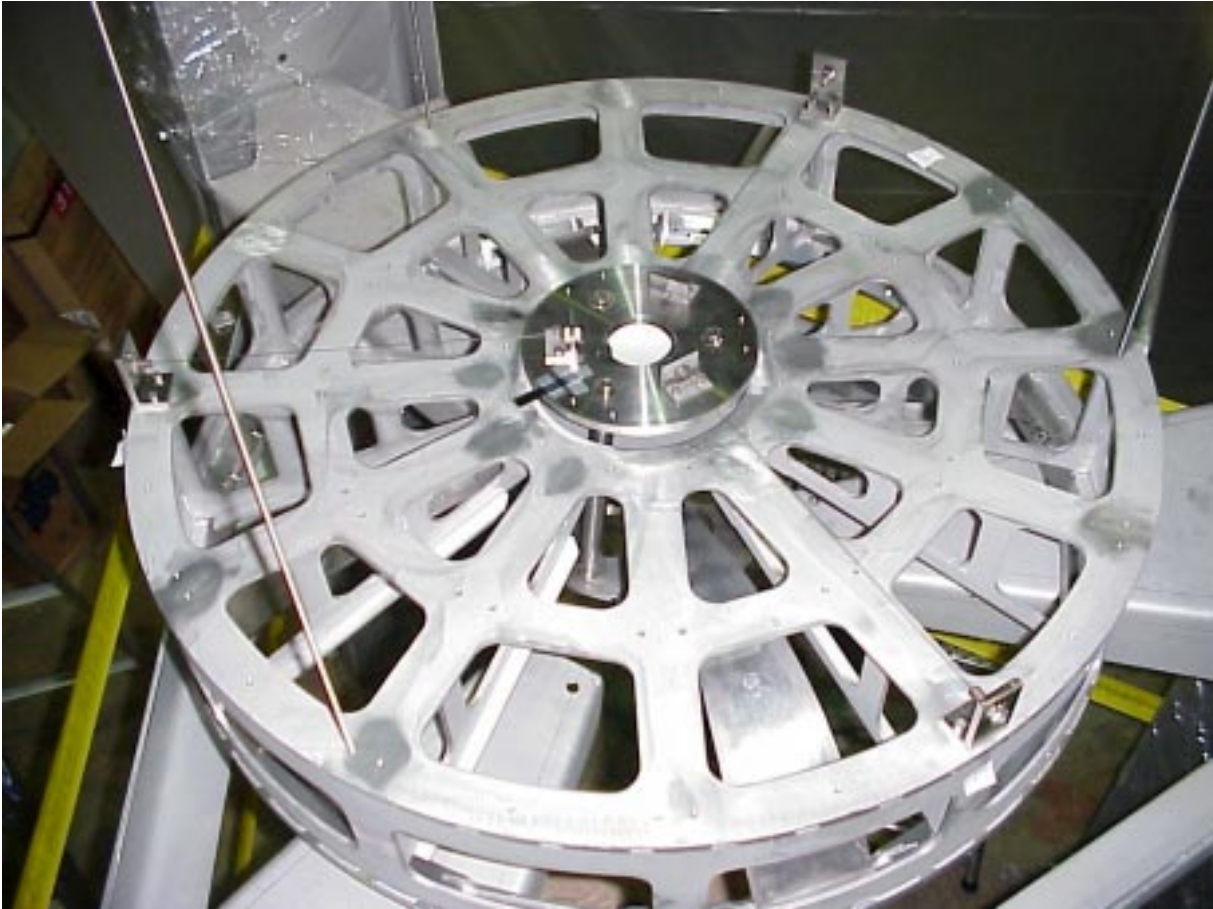


Figure 5: Picture of one of the GAS filters mounted on the test structure for the measurement of figure 3.

Vertical transfer function

Model with 6 internal blade's modes

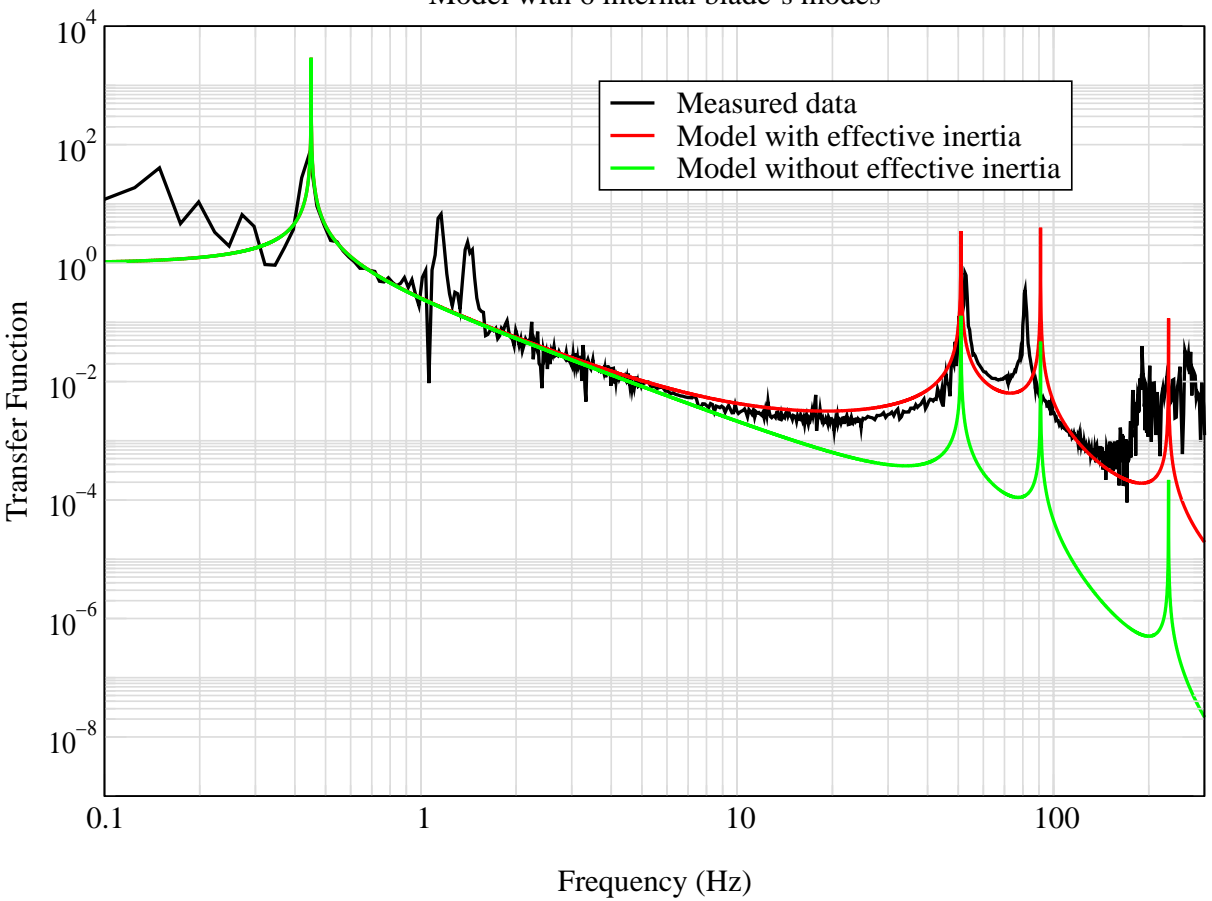


Figure 6: Measured and simulated transfer function of the GAS filter. Note the striking agreement between measurement (black) and e2e simulation (red). The GAS filter was tuned at 430 mHz and this is the only data that has been artificially input in the simulation. The $1/f^2$ behaviour flattens out at an attenuation level between 300 and 400 because of the blade mass and momentum of inertia; compare with the expected behaviour of a blade without momentum of inertia (green). The peaks above 50 Hz, not damped in this measurement, are the blade internal modes. Above 150 Hz the experimental data is dominated by the measurement noise. The two small peaks between 1 and 2 Hz are the two payload tilt modes.

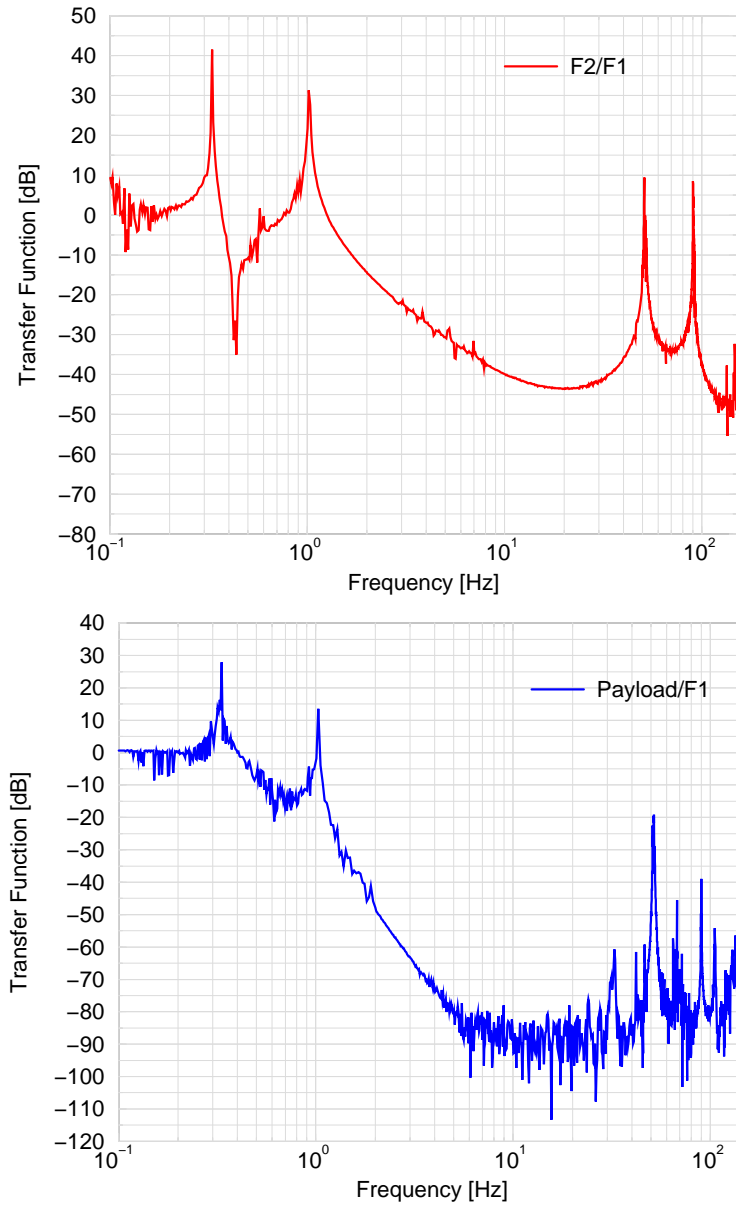


Figure 7: Preliminary measurement of the attenuation performance across 1 and 2 LIGO GAS filters in the setup of figure 9. The measurement was performed with undamped blade resonances (at 52 and 90 Hz). In filter operating conditions these resonances will be both damped and staggered (by using different blade thickness in different filters) in a real chain. This is expected to extend the more than 80dB attenuation performance to the 40 to 100 Hz region. Below the 80 dB level the measurement may be dominated by the sensor noise rather than by the residual excitation signal. The wiggles at 0.6 Hz are the filter tilt modes, which in this measurement were tuned at relatively high frequency. In normal filter operating conditions these modes would be tuned substantially at lower frequency. Tilt modes do not appear to be strongly coupled to the vertical excitation.

Vertical transfer function

Model with 6 internal blade's modes

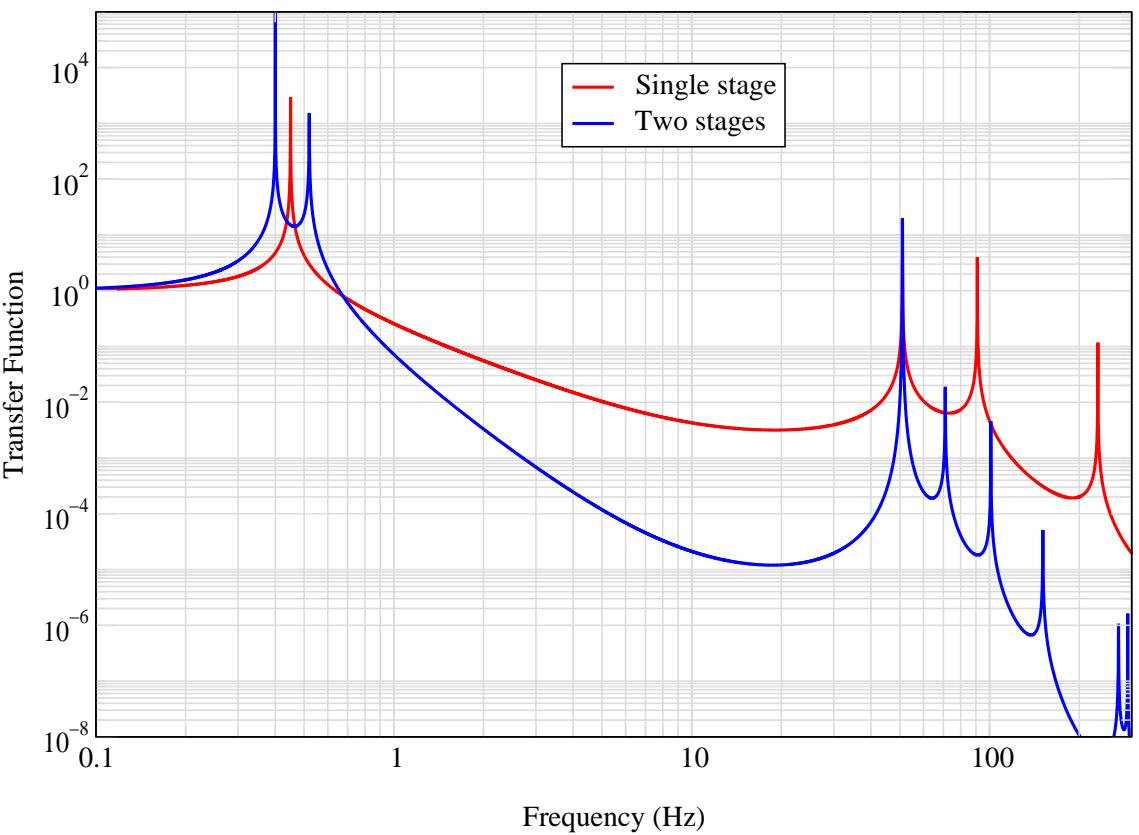


Figure 8: Simulated attenuation performance across 1 and 2 LIGO GAS filters, to be compared with measurement of figure 7. The simulation was performed with a single and two stand alone GAS filters respectively while the measurement was performed on a chain of three using the first filter (F0) as an actuator to generate the excitation. This explains the differences in behavior of simulation and experimental data between 0.1 to 2 Hz. Note the agreement of the blade's internal mode frequencies and shape, including the frequency splitting at 70 Hz in the double filter measurement. Only the blade thickness and shape was input in the simulation without further tuning. After the second blade resonance (at 90 Hz), the first common blade movement, the filter attenuation performance improves as f^{-4} power (f^{-8} for the double filter; this behavior drags all other blade resonances too low to be relevant. Only the first two resonances need to be damped to achieve the filter's nominal 40 dB attenuation at all frequencies.



Figure 9: Picture of the actual triple GAS filter chain prototype.

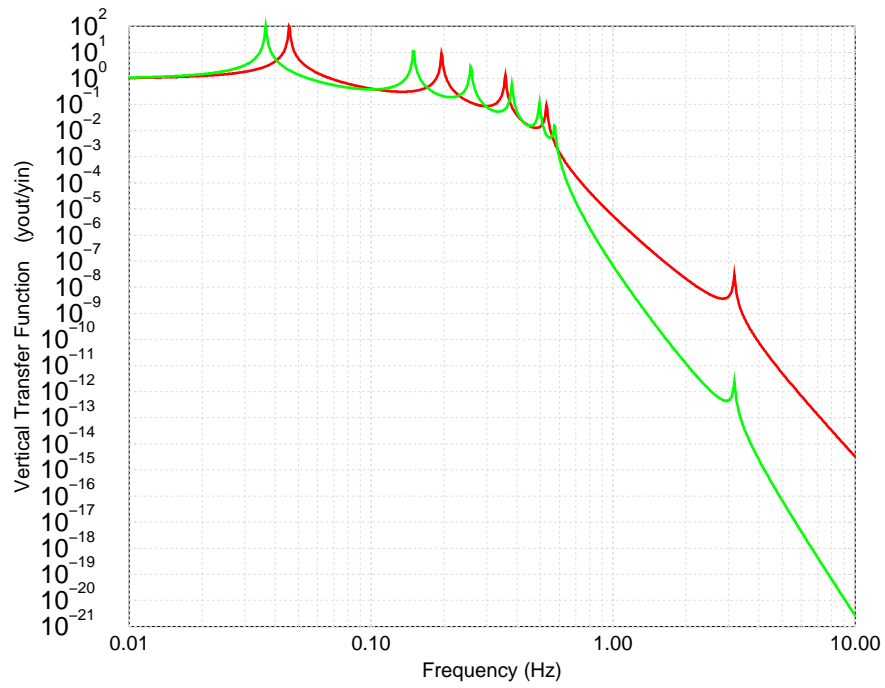


Figure 10: Vertical transfer functions of the short chain (red) and the long chain (green).

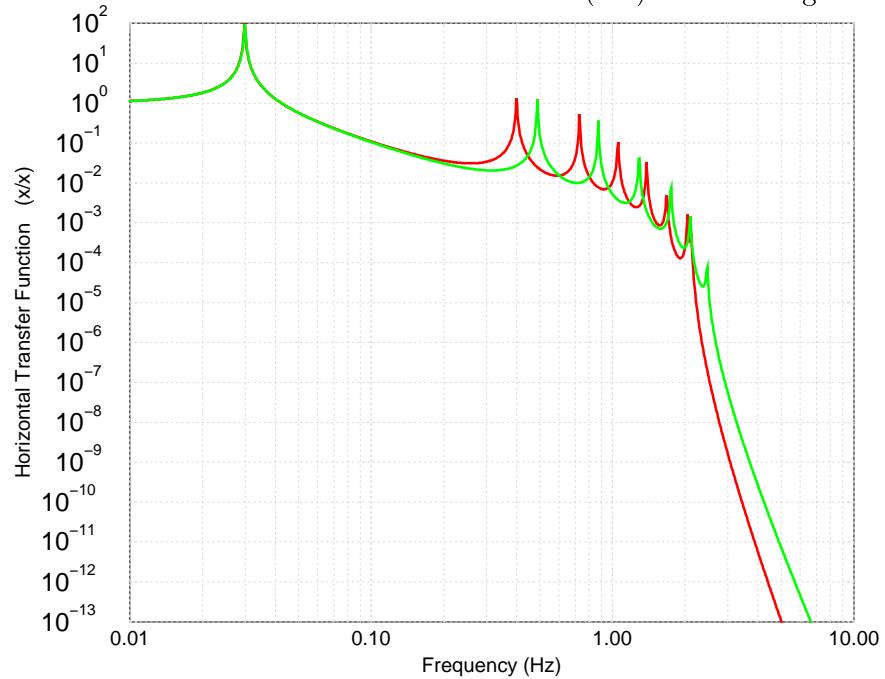


Figure 11: Horizontal transfer functions of the short chain (red) and the long chain (green).

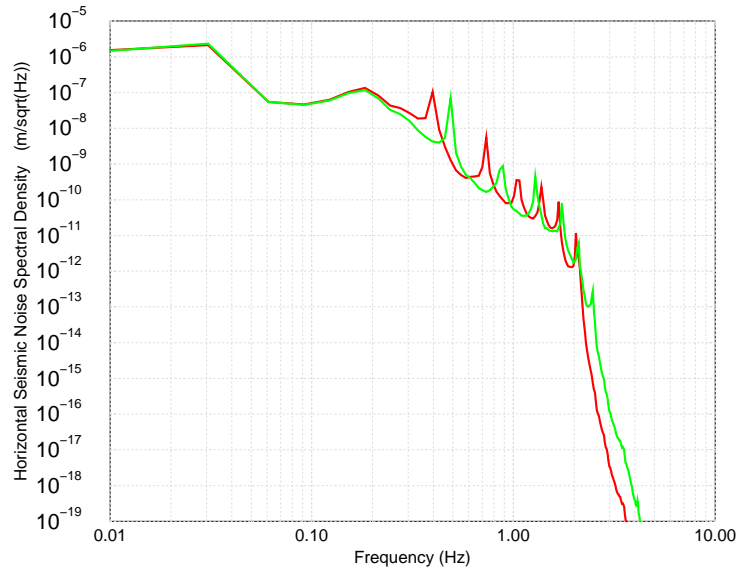


Figure 12: Horizontal seismic noise spectral density on the mirror for the tall SAS (green) and for the short SAS.

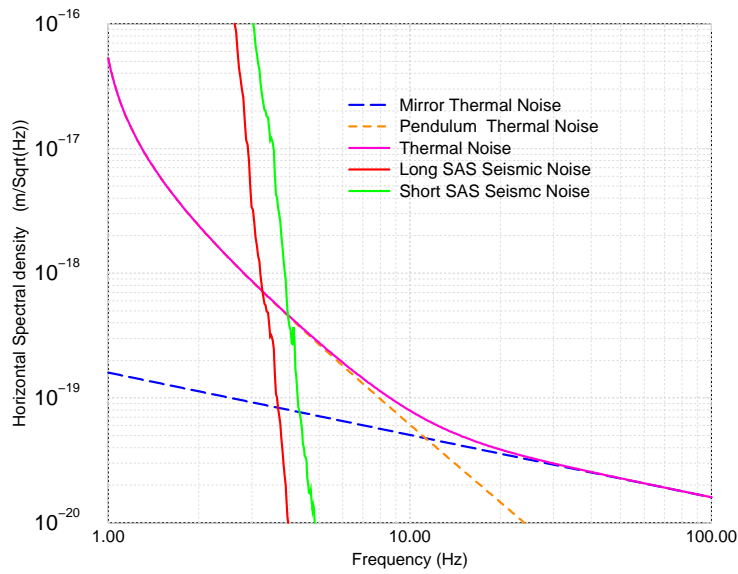


Figure 13: Particular of the horizontal seismic noise spectral density on the mirror for the long (red) and short (green) SAS compared with the mirror (blue) and ribbons pendulum (orange) thermal noise. Both SAS design easily reach the ribbons pendulum thermal noise as required.

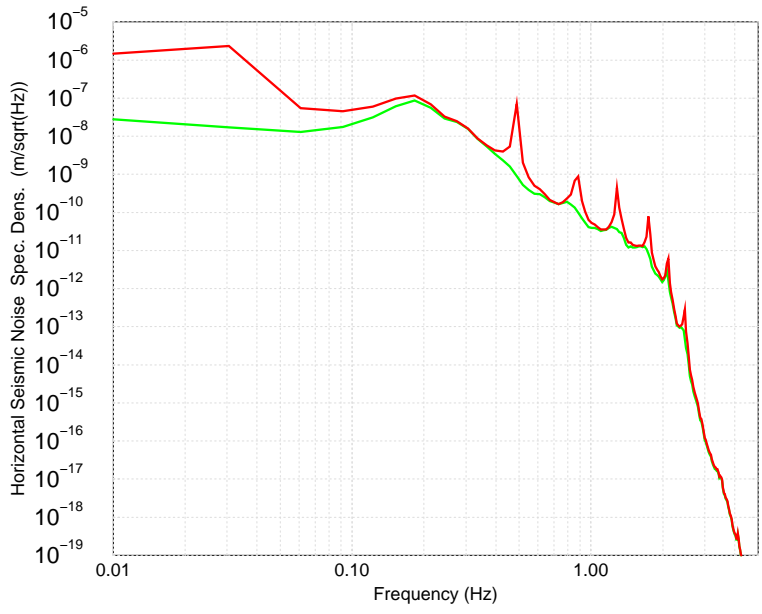


Figure 14: Horizontal Seismic noise spectral density of the mirror for the short SAS chain with and without inertial damping (blue and red respectively).

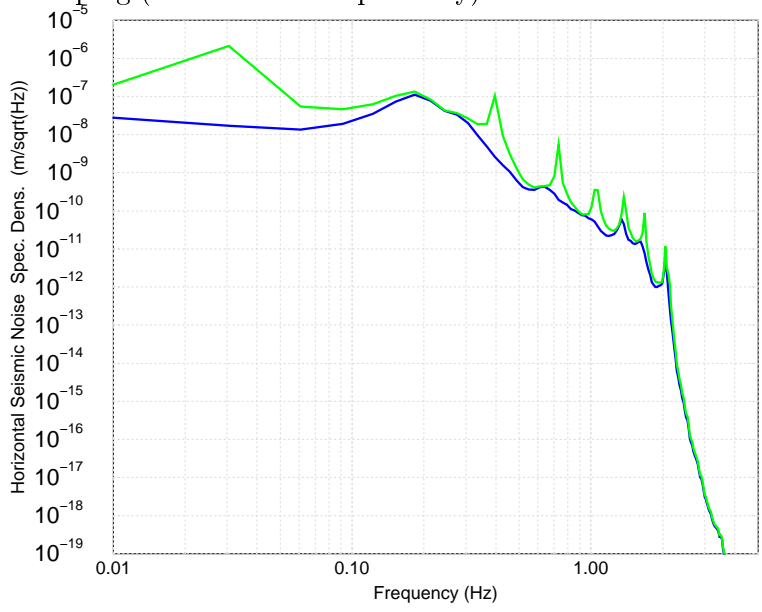


Figure 15: Horizontal Seismic noise spectral density of the mirror for the long SAS chain with and without inertial damping (blue and red respectively)..

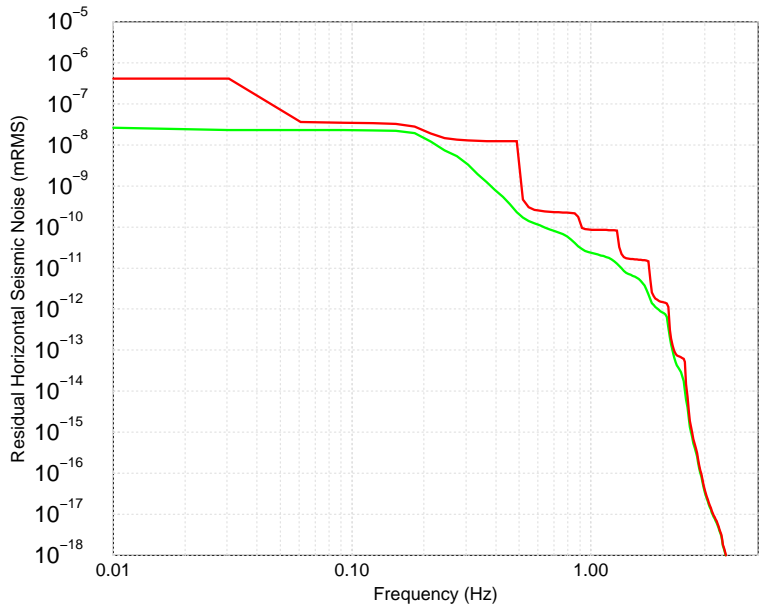


Figure 16: Integrated rms residual motion of the mirror for the short SAS chain with and without inertial damping (blue and red respectively).

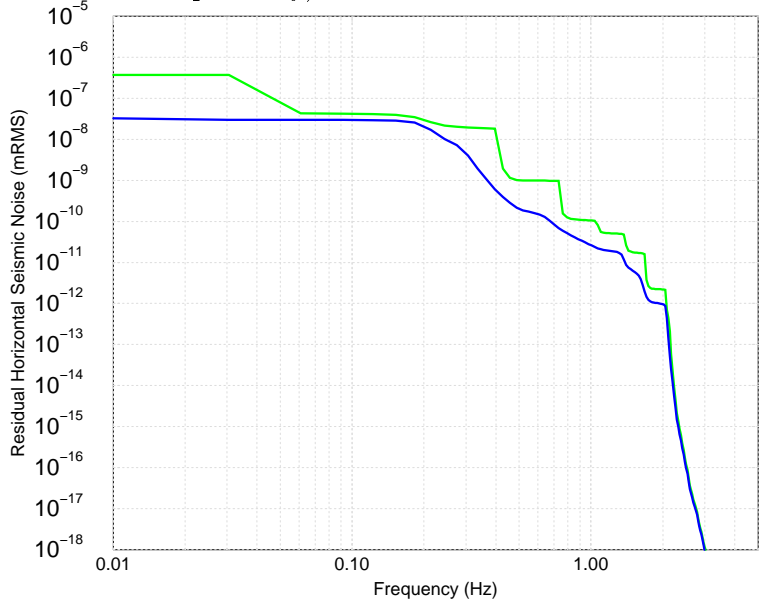


Figure 17: Integrated rms residual motion of the mirror for the long SAS chain with and without inertial damping (blue and green respectively).

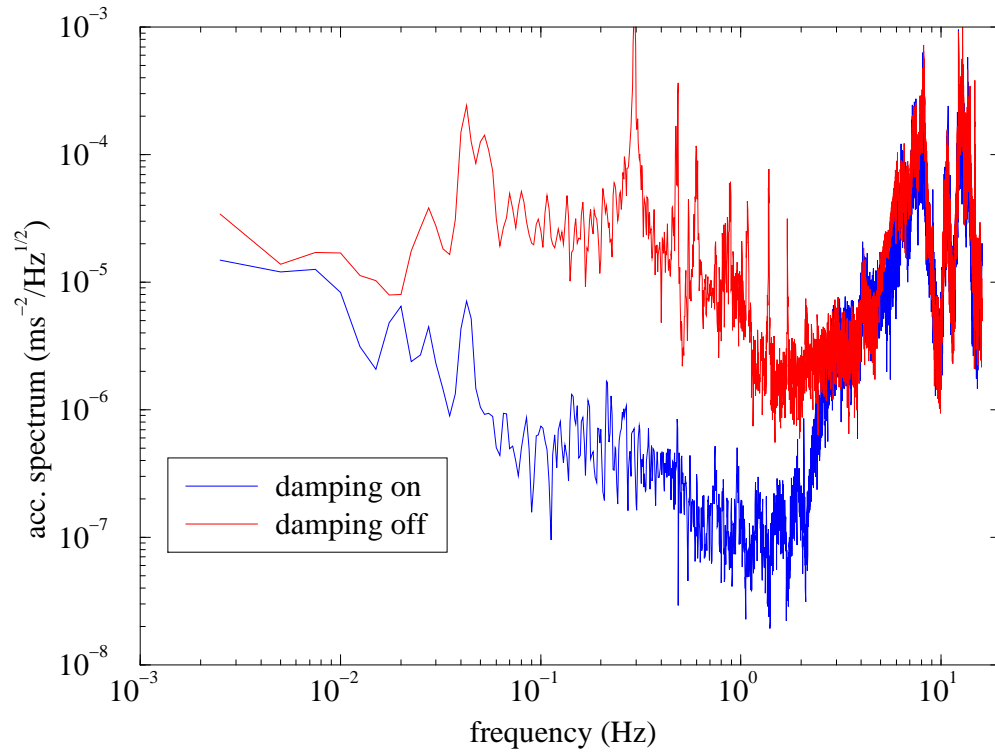


Figure 18: Effect of the inertial damping of the VIRGO Superattenuator: the horizontal acceleration is measured at the top of the inverted pendulum both with the feedback OFF and ON. A significant suppression of the seismic noise is obtained on a wide band (10mHz to 4Hz). The gain at the main Superattenuator resonance (300mHz) is about 1000 (Courtesy of the Pisa and Florence VIRGO Groups).

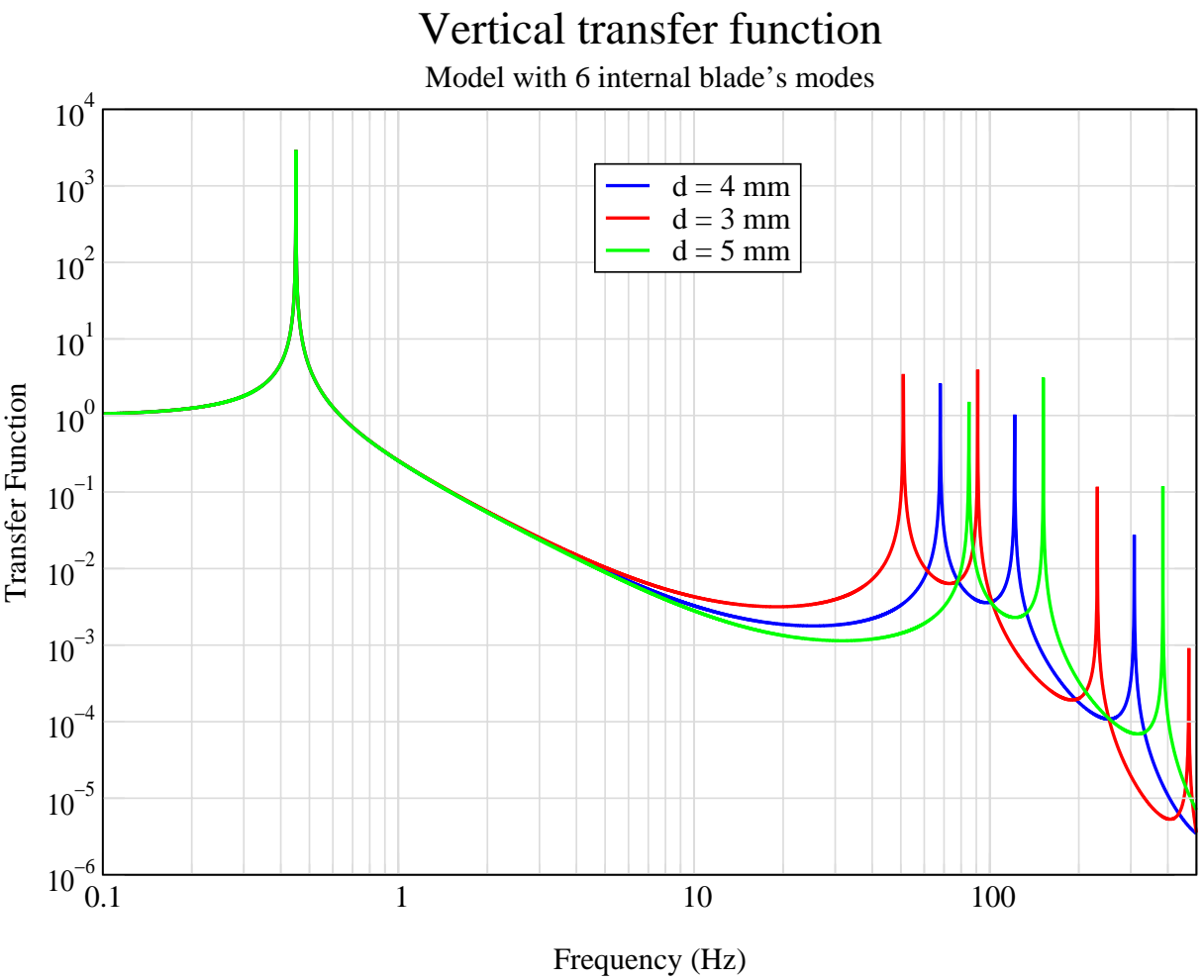


Figure 19: Effect of the thickness of the blades on the performance of the GAS filter. Thicker blades are subject to higher surface stresses, but support a given load using less blade mass. As a result the filter saturation performance bottoms out at a lower level and the blades internal resonance are pushed at higher frequency. By sequencing filters with blades of different thickness the blades resonances can be staggered in frequency thus eliminating the danger of noise paths.

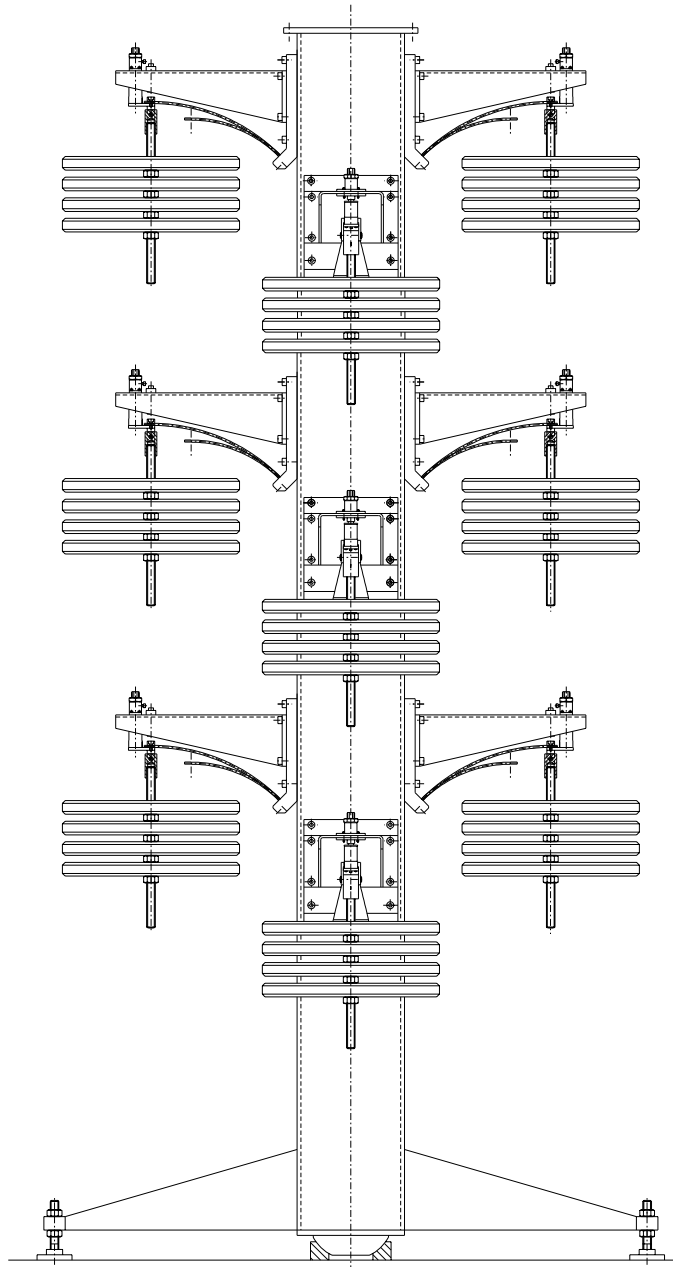


Figure 20: Schematic view of the Totem creep measurement device. Blades stressed at different levels will be tested for creep in their working configuration over the time scale of several months and at different temperatures to determine their maximum allowable stress level.

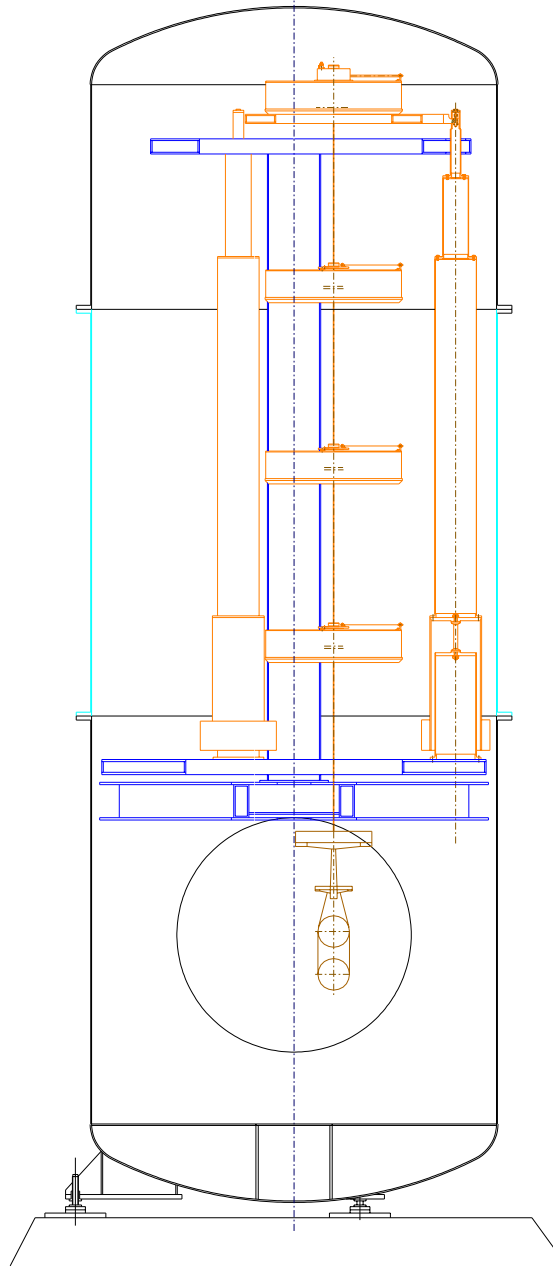


Figure 21: Offset SAS assembly The SAS structure is less than 2 m diameter, it can be easily mounted offset in the BSC towers to support interferometer mirrors off the tube axis.

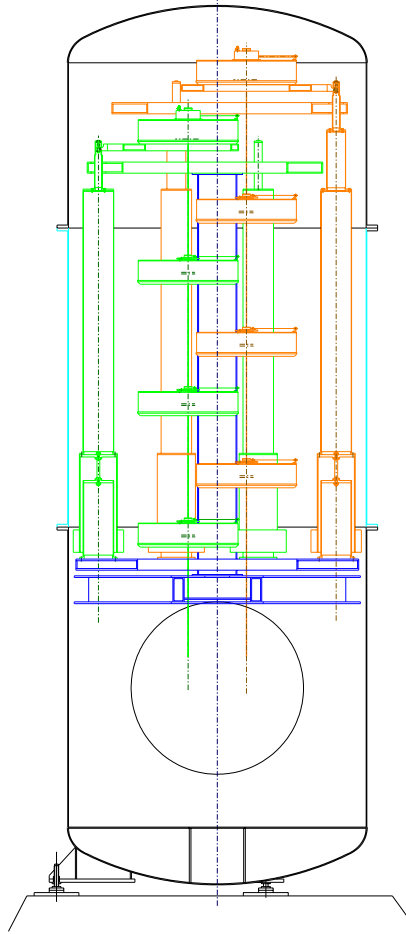


Figure 22: 2-in-1 configuration side view.(See next figure for the top view). Two independent SAS (green and orange) can fit inside the diameter of a BSC chamber (black). The safety/reference structure (blue, partially shown) in the extension pipe (light blue) is shared by the two SAS chains which are otherwise completely separated and independent.

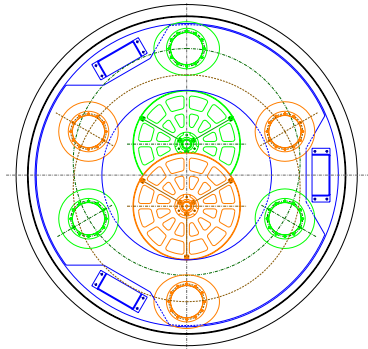


Figure 23: 2-in-1 configuration top view.

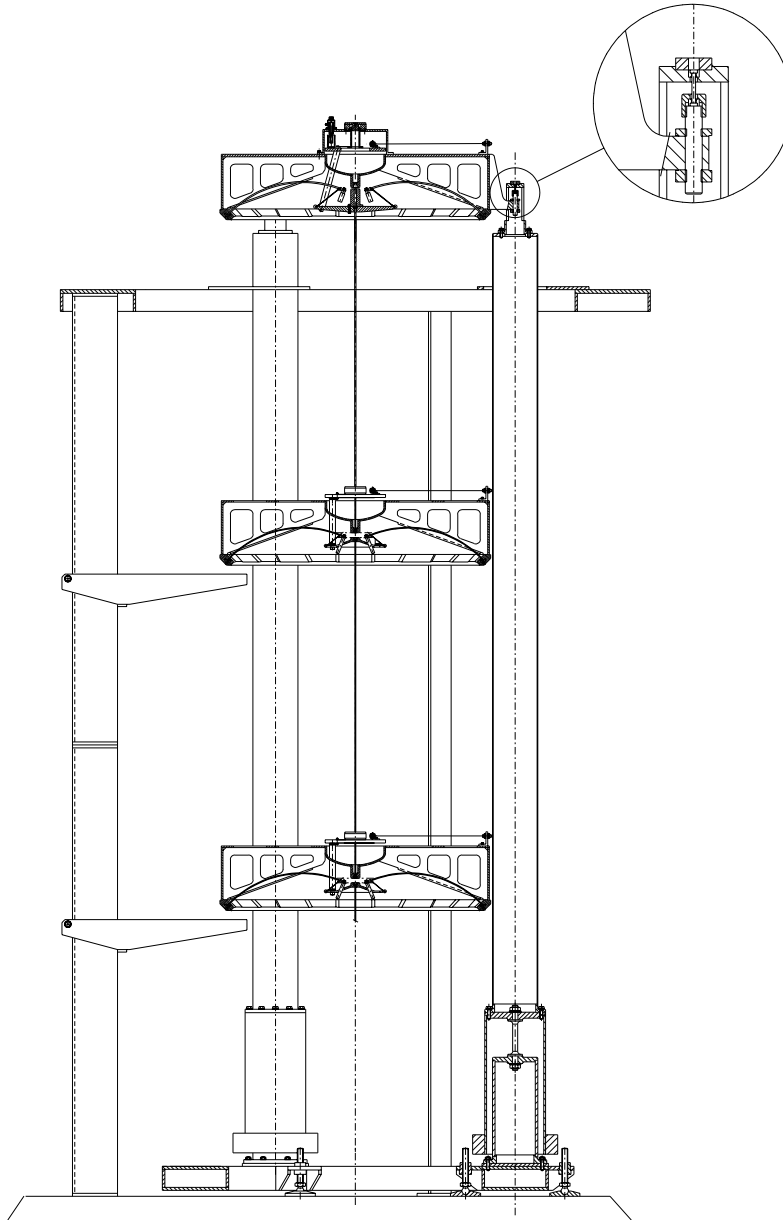


Figure 25: SAS pre-prototype being assembled in the synchrotron hall at Caltech.